Effectively Transparent Contacts for Thermally Sensitive Solar Cells using Low Temperature Reactive Silver Inks

By

Maria Kanwal

172345

Session 2016-18

Supervised by

Asst. Prof. Dr. Nadia Shahzad

A Thesis Submitted to the US-Pakistan Center for Advanced Studies in Energy in partial fulfillment of the requirements for the degree of

MASTERS of SCIENCE in

ENERGY SYSTEMS ENGINEERING

US-Pakistan Center for Advanced Studies in Energy (USPCAS-E)

National University of Sciences and Technology (NUST)

H-12, Islamabad 44000, Pakistan

December 2018

Effectively Transparent Contacts for Thermally Sensitive Solar Cells using Low Temperature Reactive Silver Inks

By

Maria Kanwal

172345

Session 2016-18

Supervised by

Asst. Prof. Dr. Nadia Shahzad

A Thesis Submitted to the US-Pakistan Center for Advanced Studies in Energy in partial fulfillment of the requirements for the degree of

MASTERS of SCIENCE in

ENERGY SYSTEMS ENGINEERING

US-Pakistan Center for Advanced Studies in Energy (USPCAS-E)

National University of Sciences and Technology (NUST)

H-12, Islamabad 44000, Pakistan

December 2018

Thesis Acceptance Certificate

Certified that final copy of MS/MPhil thesis written by Ms Maria Kanwal, (Registration No. 172345), of U.S Pakistan Center for Advanced Studies in Energy has been vetted by undersigned, found complete in all respects as per NUST Statues/Regulations, is within the similarity indices limit and is accepted as partial fulfillment for the award of MS/MPhil degree. It is further certified that necessary amendments as pointed out by GEC members of the scholar have also been incorporated in the said thesis.

Signature: _____

Name of Supervisor: Dr. Nadia Shahzad

Date: _____

Signature (HoD): _____

Date: _____

Signature (Dean/Principal): _____

Date: _____

Certificate

This is to certify that work in this thesis has been carried out by **Ms. Maria Kanwal** and completed under my supervision in Solar Energy laboratory, US-Pakistan Center for Advanced Studies in Energy (USPCAS-E), National University of Sciences and Technology, H-12, Islamabad, Pakistan.

Supervisor: _____

Dr. Nadia Shahzad
USPCAS-E
NUST, Islamabad

GEC member # 1: _____

Dr. Naseem Iqbal
USPCAS-E
NUST, Islamabad

GEC member # 2: _____

Dr. M. Parvez Akhter
USPCAS-E
NUST, Islamabad

GEC member # 3: _____

Dr. Afzal Kamboh
PCRET
Islamabad

HoD- (dept) _____

Dr. Naseem Iqbal

Principal/ Dean _____

Dr. Zuhair S. Khan
USPCAS-E
NUST, Islamabad

Abstract

There is great interest in minimizing the various losses caused by metal contacts in photovoltaic devices, in particular the optical and shadowing losses. In this study, a polymeric Polydimethylsulfoxide (PDMS) mold inscribed with a triangular microchannel pattern is used to deposit front metal contacts using a highly conductive, low temperature reactive silver ink (RSI) via capillary action. Fingers deposited with this technique exhibit a high aspect ratio, are optically narrow and ~ 85 % transparent. The resulting effectively transparent metal contacts (ETCs) can redirect incoming solar radiation to the photo-active area of the solar cell and mitigate parasitic absorption as well as shading losses. The use of RSI for the development of (ETCs) at low processing temperatures makes it possible for optoelectronic devices to include thermally sensitive layers. RSI exhibits high conductivity which is comparable to that of bulk silver if uniform films are deposited and anneals at ~100°C, making it suitable for devices that require low temperature processing. With the reduction of porosity upon addition of a suitable solvent and increasing compactness of these grid effectively transparent contact grid fingers, they have the potential to outperform their low temperature silver paste screen-printed counterparts in terms of both cost and efficiency and could even replace TCOs altogether.

Keywords: Effectively transparent contacts, Reactive silver ink, Perovskite solar cells, low temperature metallization, Photovoltaics.

Table of Contents

List of Figures

List of Tables

List of Conference/Journal Papers

1. Maria Kanwal, Nadia Shahzad, Salman Manzoor, *"Effectively transparent contacts with low temperature reactive silver ink"*. Published in proceedings of the International Conference on Renewable, Applied and New Energy Technologies, at AIR University, Islamabad, Pakistan.

Chapter 1: Introduction

1.1 Energy requirements

With the rapid increase in the demand for energy in the industry, transportation and domestic sector, it is becoming more and more difficult meet the requirements. The energy requirements are expected to expand further by as much as 30% by the year 2040 [1]. Rapid development in technology, especially in the field of renewable energy will help overcome some of the barriers to adequate, efficient and environment friendly energy production. With the recent interest in environmental impact of carbon-based energy sources and their contribution towards climate change as reported by environmental agencies, the attention has been shifted dramatically to renewable energy resources, which promise a clean, green alternative to the conventional carbon-emitting fuels. Among the few adverse health effects of using fossil fuels are respiratory, skin and eye diseases. The release of CO2, SOx and NOx into the air as a result of burning fossil fuels also causes acid rain and smog which damage the environment and lead to various health problems.

1.2 Global warming and climate change

Huge amounts of the major green-house gas are produced by burning coal, oil and natural gas, contributing significantly to global warming which is believed to be occurring at a rate of 0.13°C per decade. The Earth's average surface temperature has risen by about 0.9 °C since the late nineteenth century due to dramatic rises in atmospheric CO_2 and other man-made emissions. 2016 was recorded as the warmest year, with 8 of the 12 months showing temperatures higher than ever recorded before. With the ever-growing need for energy production and collateral damage caused by the emissions released as a result of conventional energy production technologies, there is a constant ongoing search for alternative means of fulfilling global energy demands. According to the World Energy Outlook 2017, two of the four large scale shifts in the global energy system include 1) rapid deployment and decrease in prices of green energy technologies 2) rapid electrification of energy.

1.3 Global warming and climate change

Over the past few years, the share of renewable energy sources in global electricity consumption has doubled. The global dependence on renewable resources, mainly wind and solar in the year 2011 was around 19% and these two renewable energy

sources accounted for almost 36% of the total global electricity generation in 2015, a 17% expansion during a period of five years. Dissemination of renewable sources of energy depends on multiple factors like increasing technology efficiency, decreasing rates, government policies and unreliability of fossil fuels. Renewable energy technologies like photovoltaics, solar thermal, biofuels, wind energy and hydroelectric have the potential to fill the energy demand-supply gap. However, for these technologies to be viable, they should be affordable, efficient and environment friendly. Of all the possible alternatives to conventional energy technology, solar energy seems to be the most reliable and affordable choice. Received in abundance by the earth (23,000 TW per year), solar energy can help decrease our dependence on carbon-based fuels and gradually ameliorate the threat of global warming. According to the World Energy Outlook 2017, renewable sources are expected to capture 2/3rd of the global investment on power plants by 2040, as they will soon become the most affordable sources of electricity generation in many countries [1].

1.4 Energy mix of Pakistan

Pakistan's energy mix relies heavily on imported fuel which makes up for around 40% of total imports in the country, contributing greatly to a cumbersome current account deficit. For an economy to grow sustainably, electricity production should be equal to or exceed the GDP growth rate, however, the gap between supply and demand increases each year. Pakistan generated some 34 percent of its total electricity from natural gas, roughly 31 percent from oil, 26 percent from hydro, almost 6 percent from nuclear and a mere 2 percent from renewable energy resources in 2017 [1]. Large amounts of coal are also being imported now for many new coal-based power plant projects. There is a dire need for this energy mix to be skewed towards Pakistan's indigenous resources, with a keen focus on the renewable energy sector. In terms of solar potential, Pakistan is at advantage due to its geographical location, with an annual solar irradiance of 1,900-2,200 kWh/m^2 and an estimated solar power potential of 2,900 GW [2]. According to estimates by NEPRA and IEEFA, wind and solar are now among the cheapest sources of energy in Pakistan [3].

1.5 Global solar atlas

The Global *Solar* Atlas provides information about the solar power potential and solar resources for different regions in the world [2]. This can be used to carry out

an electricity output calculation at any desired location that is covered by the solar resource database.

1.6 Solar technologies

1.6.1 Solar thermal technology

Solar thermal energy has been used by ancient people for centuries, to utilize heat from the sun for heating and drying purposes. A more recent development has brought about interest in the use of thermal processes for power generation, water purification, mechanical crop drying and water heating [4] . According to the range of temperatures acquired, solar thermal technology can be used for the following purposes;

- Temperatures lower than 100 ºC are required for water heating or air conditioning for domestic purposes, evaporative techniques like distillation, in dryers and swimming pools etc.
- Cooling and heating of water, air or oil for industrial purposes and air conditioning for homes and buildings requires temperatures around 150 ºC.
- Temperature in the range of 200-2000 ºC are needed for the generation of mechanical and electrical power.
- For use in solar furnaces to treat materials, temperatures up to 5000ºC are needed.

There are two types of solar thermal systems, an active solar thermal system and a passive solar thermal system. For a passive system, no special equipment is required e.g. when heat is trapped and builds up inside a car when left out in the sun. An active system, however, requires a means to absorb, collect and then store solar radiation.
Solar thermal power plants are active solar thermal systems which can be of many different kinds depending on its structure and working. There are many basic similarities in all such systems in terms of the individual components. Receivers collect solar energy for conversion thermal energy, mirrors are used to reflect and concentrate the incoming sunlight and a generator is used to produce the heat generated from this system.

1.6.2 Solar photovoltaics

Around one third of the total world population lives in rural areas with no access to the main electricity grid. Solar energy, which is present in abundance and is among the

cleanest resources that holds great promise for fulfilling the global energy demand. However, a few major challenges need to be overcome to make this technology more economically favorable. Among the multiple sources of renewable energy technology, PV energy power systems hold the most dominant and successful position. Based on many studies on the future of the global energy mix, it is evident that solar energy will hold one of the greatest shares. The reasons for its attractiveness include, but are not limited to, zero carbon emission, zero noise pollution, scale flexibility, longevity and simplicity in maintenance and operation [5]. The International Energy Agency (IEA) envision that solar electricity will make up for somewhat around 20% of the total global energy production by the year 2050, in which PV systems will play a major role. This means that in the years to come, there will be a tremendous amount of focus on developing the PV industries and overcoming the few hurdles faced by it [6].

During the initial phase of this technology, production of a single PV panel required more energy than the output it would give during the entire course of its lifetime. But in the past few years it has undergone great advancements such that record efficiency devices have been developed with improved manufacturing methods, reducing the payback period to 3 to 5 years [5]. The electricity generated by PV energy systems may be used for a variety of applications, from power supplies for small consumer applications to large power stations, feeding electricity into the grid. Growth rate of the world photovoltaic industry is approximately 49.5% over a period of 5 years. In 2008, the world solar photovoltaic (PV) market reached a record of installations of 5.95 gwatts (GW), exhibiting a growth of 110% over the course of one year.

1.6.3 Working of a solar cell

A solar cell is a an electrical device that converts sunlight energy directly into electricity, due to a phenomenon called the photovoltaic effect. Converting this sunlight into electrical energy requires a semiconducting material to absorbs the solar radiations (in the form of photons) which causes the release of and electron to a higher energy state, from where it is made to flow through an external circuit. Silicon is one such material that exhibits this phenomenon.

Photovoltaic cells are arranged to form a PV module which are in turn connected in series and then parallel configuration to form an array. The output direct current (DC) is then converted into alternating current (AC) for use by nearby buildings or Is

exported to the electricity grid. One of the biggest advantages of this technology is the ease in scalability, with system sizes ranging from 2-10 kW for domestic purposes, 100-500 kW for commercial and greater than 10 MW for utility scale. Distribution plants of >100MW are also being currently built [7].

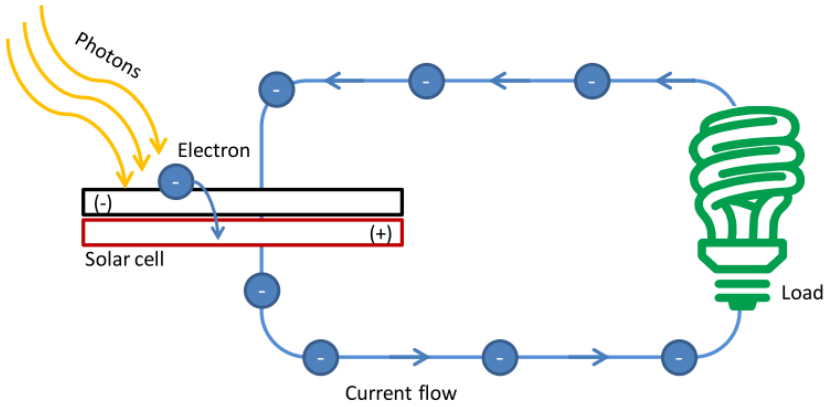

Figure 1. Schematic diagram of photovoltaic device

1.7 Types of photovoltaic solar cell technologies

Owing to the rapid advances and vigorous research in this area, many new types of semiconducting photovoltaic materials have been developed in addition to the traditional Silicon based solar cells. PV technologies are divided into three generations.

1.7.1 First generation solar cells

Conventional solar cells are manufactured using silicon which is found in huge abundance on the Earth and is nontoxic. The silicon solar cell market has boomed ever since its inception and it continues to be the leading technology, making up for around 90% of the total generated revenue[3]. This is because it is a reliable and well-demonstrated technology with the highest power conversion efficiencies consistently for over 30 years in the field. Degradation in performance and reduction in generated power after long-term exposure is less than 1% per year. Silicon modules have the longest lifespan, up to 25–30-years but they can still keep generating electricity beyond this range. Silicon solar cell technology is predominantly based on two kinds of cells, monocrystalline (single junction) and multicrystalline (polycrystalline) solar cells that are classified on the basis of crystal size and number of grain boundaries, which can be controlled by choice of raw material and fabrication technique. The theoretical limit imposed on the efficiency of monocrystalline solar cells under standard test conditions,

as determined by Shockley and Queisse is 30%. The highest solar efficiency measured for Monocrystalline solar cells in the lab was 26.1% in the year 2018 [8]. Typical overall efficiency of single crystal silicon solar panels is around 18%. However, some of the leading manufacturers of monocrystalline solar cells claim an overall efficiency of around 22% for their panels [4].

1.7.2 Second generation solar cells

In an effort to reduce the manufacturing and material cost of solar cells, many advances have been made in thin film technologies that led to the development of novel photovoltaic materials like Cadmium Telluride (CdTe), Amorphous Silicon heterojunction and Copper Indium Gallium diSelenide (CIGS). Thin film technologies such as PVD, CVD, PECVD and sputtering have been used to deposit these materials, which show comparatively lower efficiencies than first generation solar cells. The highest efficiency is measured for CIGS so far is 22.9% [8] which is not that far off from that of single crystal silicon solar cells. The biggest advantage of this generation of solar cells over silicon solar cell technology is the ease of fabrication with precise control and reduction in fabrication cost. These cells are only a few micrometers thick. Due to their small thicknesses, these semiconducting materials can find application in flexible PV devices [9]. The efficiency of thin-film solar cells is generally lower than for crystalline cells. The current efficiency of a thin-film a-Si heterojunction solar cell is 14% and 22.1% for CdTe solar cell [8].

1.7.3 Third generation solar cells

This generation of solar cells is based on organic, inorganic and hybrid solar cells fabricated using solution processing techniques e.g. perovskite solar cells (PSCs) [10], dyes sensitized solar cells (DSSCs) and organic solar cells (OPVs). These cells generally show low efficiencies but are the center of attention in current photovoltaic research due to the low material and fabrication costs [11]. The highest record efficiency obtained with perovskite solar cells thus far is 23.3% and 12.9% for organic solar cells, whereas that for dye sensitized solar cells is still only 11.9% [8]. Perovskites hold great promise as an emerging technology and are being coupled with silicon and other solar cells to for high efficiency tandem devices at a world record efficiency of 25.3% [12], [13].

1.8 Types of losses in third generation

Identifying the causes of efficiency loss is crucial to improving the solar cell performance by coming up with a well thought through strategy. The mechanisms of energy loss in perovskite solar cells mainly include i) below bandgap loss ii) optical loss iii) recombination loss iv) thermalization loss v) spatial relaxation loss.

1.8.1 Below bandgap loss

When photons with lower energy than that of the absorber layer band gap fall on to it, they fail to generate electron/hole pairs. These photons do not contribute to generation of electricity and are wasted. The below bandgap loss can be presented as

$$Q_{belowEg} = \int_0^{Eg} E_\lambda PFD_{AM1.5}(E_\lambda) dE_\lambda$$

1.8.2 Thermalization loss

Photons with energy greater than the bandgap energy of the semiconducting material can generate electron/hole pairs with high kinetic energy. These high energy charge carriers, however, relax back to their state of thermal equilibrium with the release of excess energy by interacting with the crystal lattice through a process called thermalization. The amount of energy lost in bringing the excited charge carrier into equilibrium accounts for the thermalization loss.

1.8.3 Optical loss

Optical losses arise from phenomena such as transmission, reflection and parasitic absorption leading to a loss in the number of photons absorbed by the device[14]. It refers to photons that have energy higher than the bandgap but are not effectively absorbed by the photoactive material. Can be expressed as

$$Q_{optical} = \int_{Eg}^{\infty} E_\lambda PFD_{AM1.5}(E_\lambda) dE_\lambda$$

1.8.4 Recombination loss and Spatial relaxation loss

Both the spatial relaxation and recombination losses are caused by the carrier annihilation that takes place during the process of charge transport. Hence, they are both classified as electrical losses. Some of the photogenerated charge carriers may undergo recombination while being transported to the charge collection layers. When

the photogenerated carriers lose potential energy while jumping from the band edge to contacts[14].

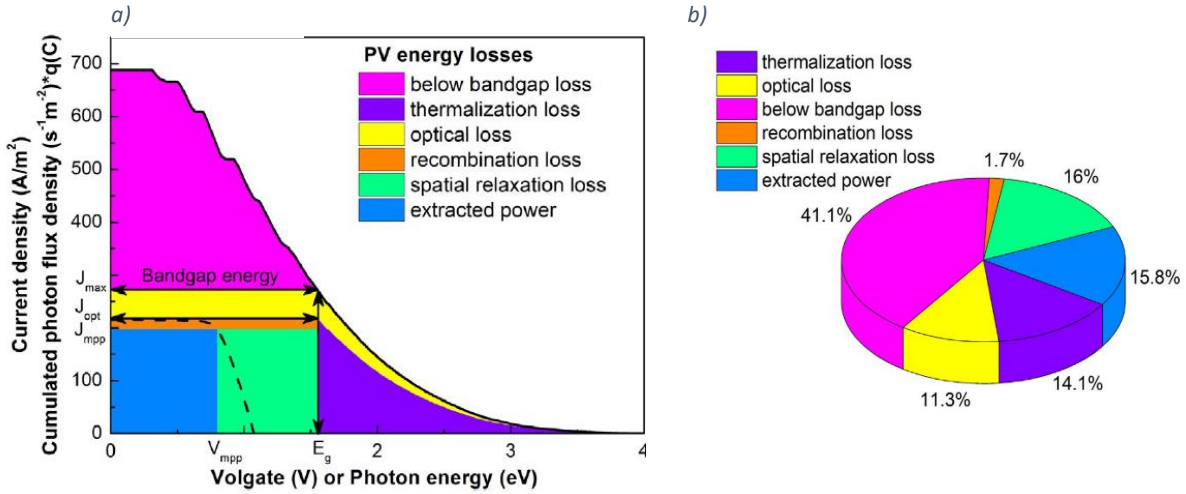

Figure 2 a) Energy loss occurring in the perovskite solar cells b) Quantifying energy losses in perovskite solar cells under A.M 1.5 conditions (14)

Fig 2. Shows the solar radiation incident on the cell, represented by the total area. The various energy losses are caused by multiple different phenomena and are represented by the colored regions. Below band gap losses make up for the major percentage of the total energy loss PVK solar cells. This is attributed to the fact that PVKs have a large bandgap (Eg = 1.55 eV) which limits the photons that are effectively used.

1.9 Optical and electrical losses as extrinsic losses

Thermalization and below bandgap losses are intrinsic in nature, making them pretty much unavoidable. This leaves us with the extrinsic losses that can be removed to some extent feasibly. This can be done by focusing on improving the optical and electrical properties of these devices [14]. Optical loss in PVKs consist of reflection, transmission and parasitic absorption leading to a loss in the number of photons absorbed by the device which cause a decrease in short-circuit current density (J_{sc}) and the power conversion efficiency of the cells. It is evident from fig 2. b) that optical losses in PSK solar cells is responsible for 11.3% of the total incident solar radiation. The band gap of Cs based perovskites is around 1.73 eV, so optical losses in the wavelength range of 300-800 nm. Fig 3. shows optical losses in terms of equivalent current density as determined from the absorption spectrum. Moreover, the reflection loss is 2.48 mA/cm^2 whereas the total parasitic loss is 3.48 mA/cm^2. These two losses

account for the major fraction of lost incident light in perovskite solar cells. Suggesting that optical optimization of device design is crucial to improving performance in these cells.

1.9.1 Reducing optical losses (and resistive) in solar cells (losses in front metal grid)

- Antireflective coating may be deposited on the top surface of a cell
- Nanostructures that serve as an antireflective textured surface can also reduce reflection losses
- Reducing TCO thickness to reduce parasitic absorption but increase sheet resistivity
- Combination of light trapping and surface texturing can be used to increase path length of light

- Shading loss at the front metal grid - (SHJs) amounts to 2.8mA/cm2 that is ~6%. Metal contacts with higher aspect ratio can reduce shading losses [5]

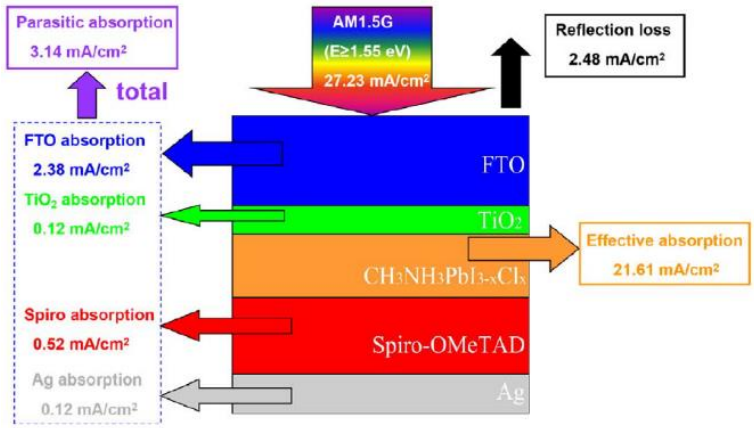

Figure 3 Quantifying optical losses in PVK solar cells (14)

The solar cell series resistance consists of multiple components as shown in the diagram below, of which the emitter and top grid resistance dominate the overall series resistance and are therefore most heavily optimized in solar cell design. Grid resistance consists of the finger and busbar resistance.

1.9.2 Resistive losses in metal grid

A metallic top contact is required in solar cells for collecting the current produced by the semiconducting material in the solar cell. A typical solar cell has a metal grid made of multiple hair thin fingers that run across the length of the cell. These fingers are tapered towards the end and are connected to the external circuit by means of thicker busbars. There exists a trade-off between the resistive losses associated due to the largely spaced fingers and increased reflection owing to the huge amounts of metal covering the top surface of the cell [15].

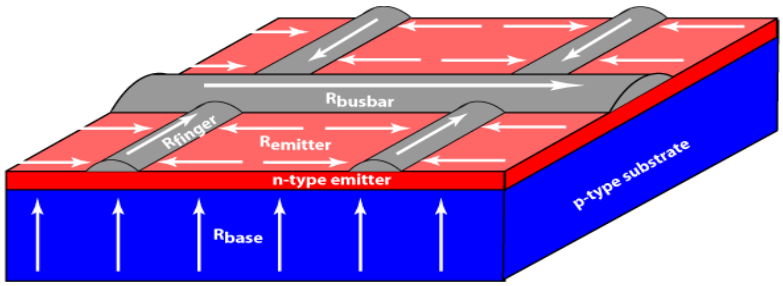

Figure 4. Resistive losses and current flow in a solar cell

1.10 Summary

This chapter discusses the significance of renewable energy and the solar potential of Pakistan. Focusing on the solar photovoltaic technology, the various generations of solar cells and have been overviewed i.e. the first generation, which includes predominantly mono and multi-crystalline silicon wafer based solar cells; second generation solar cells that are fabricated using vacuum based technologies to form thin layers in the nano to micro meter range e.g amorphous silicon, Cadmium Telluride (CdTe) and Copper Indium Gallium diSelenide (CIGS); and the third generation of solar cells, which include solution processed Dye sensitized solar cells (DSSCs), perovskites (PVKs) and Lead Lanthanum Zirconium Titanate (PLZT). Various losses incurred by the third-generation solar cells and the underlying mechanisms are described in detail with a particular focus on the optical and electrical losses caused by the top metal contact. It is evident that the various losses incurred due to the metal contacts reduce the power conversion efficiency of the solar cell. Hence, a metal grid design that offers minimal shading, reflective, parasitic absorption and resistive losses should prove effective in overcoming these challenges.

References

[1] A. H. Khan, "No Title," *Dly. Pakistan J.*, 2018.

[2] M. M. Ra, S. Rehman, and S. Asia, "National energy scenario of Pakistan – Current status , future alternatives , and institutional infrastructure : An overview," vol. 69, no. October 2015, pp. 156–167, 2017.

[3] H. B. Khalil and S. J. H. Zaidi, "Energy crisis and potential of solar energy in Pakistan," *Renew. Sustain. Energy Rev.*, vol. 31, pp. 194–201, 2014.

[4] "Solar Thermal Systems ©," 2012.

[5] F. Diner, "The analysis on photovoltaic electricity generation status, potential and policies of the leading countries in solar energy," *Renew. Sustain. Energy Rev.*, vol. 15, no. 1, pp. 713–720, 2011.

[6] J. Salasovich and G. Mosey, "Feasibility Study of Economics and Performance of Solar Photovoltaics at the Refuse Hideaway Landfill in Middleton , Wisconsin A Study Prepared in Partnership with the Environmental Protection Agency for the Feasibility Study of Economics and Performance ," no. August, 2011.

[7] J. Simon and G. Mosey, "Feasibility Study of Economics and Performance of Solar Photovoltaics at the VAG Mine Site in Eden and Lowell , Vermont A Study Prepared in Partnership with the Environmental Protection Agency for the RE-Powering America ' s Land Initiative : Siting Renew," no. April, 2013.

[8] National Renewable Energy Laboratory, "Https://Www.Nrel.Gov/Pv/Assets/Pdfs/Pv-Efficiencies-07-17-2018.Pdf," p. accessed on July 24, 2018, 2018.

[9] H. Tan *et al.*, "Efficient and stable solution-processed planar perovskite solar cells via contact passivation," *Science (80-.).*, vol. 355, no. 6326, pp. 722–726, 2017.

[10] W. S. Yang *et al.*, "High-performance photovoltaic perovskite layers fabricated through intramolecular exchange," *Science (80-.).*, vol. 348, no. 6240, pp. 1234–1237, 2015.

[11] M. R. Leyden, Y. Jiang, and Y. Qi, "Chemical vapor deposition grown formamidinium perovskite solar modules with high steady state power and thermal stability," *J. Mater. Chem. A*, vol. 4, no. 34, pp. 13125–13132, 2016.

[12] K. A. Bush *et al.*, "23.6%-Efficient Monolithic Perovskite/Silicon Tandem

Solar Cells With Improved Stability," *Nat. Energy*, vol. 2, no. 4, pp. 1–7, 2017.

[13] G. E. Eperon *et al.*, "Perovskite-perovskite tandem photovoltaics with optimized band gaps," *Science (80-.).*, vol. 354, no. 6314, pp. 861–865, 2016.

[14] Y. Da, Y. Xuan, and Q. Li, "Quantifying energy losses in planar perovskite solar cells," *Sol. Energy Mater. Sol. Cells*, vol. 174, no. January, pp. 206–213, 2018.

[15] J. Bullock *et al.*, "Microchannel contacting of crystalline silicon solar cells," pp. 1–8, 2017.

Chapter 2: Literature Review

2.1 Optimizing metal grid design

Not all of the incident light falling on the solar cell does reaches the absorber layer because it has to pass through many of the preceding layers that incur multiple losses. Parasitic absorption occurring at the TCO accounts for much of the loss in radiation, reflection at the top metal contacts and shading losses due to the metal fingers further reduce the amount of light reaching the absorber layer. Other than these optical losses, resistive losses at each interface, particularly the metal grid, also reduce the solar cell performance to some extent. Shading loss at the front- (SHJs) amounts to 2.8 mA/cm^2 that is ~6% [1]. Introducing a metal grid in addition to a TCO layer would improve charge collection, however, the transparency of the grid should be significantly high to avoid reductions in the light harvesting and the material used for this grid should be highly conductive, with conductivity values comparable to silver [2].

2.1.1 Emitter resistance

The power loss caused by the emitter resistance can be determined by the pitch of the fingers in the top contact. However, the distance travelled by the current in emitter varies. Current collection can take place from the base of the emitter and hence only has a small distance before it reaches the finger, or it can enter the emitter in between the fingers, in which case the length of the path is equal to half the spacing between individual fingers. The fractional power loss in emitter is reduced by decreasing the spacing between the fingers, but there is always a trade of between resistive and optical losses when designing the fingers.

2.1.2 Contact resistance

This loss occurs at the interface between the metal contact and solar cell. In case of perovskite solar cells, it occurs between the TCO and the charge transport layer. For 1^{st} and 2^{nd} generation solar cells, a metal grid is deposited to collect charge from the solar cell and transfer it to the external circuit. The contact resistance loss at various points at the interface between metal grid and semiconducting material is different. Solar cell contact resistance can be measured in a number of ways. One such method involves biasing the cell at maximum power point and measuring voltage drops across the cell.

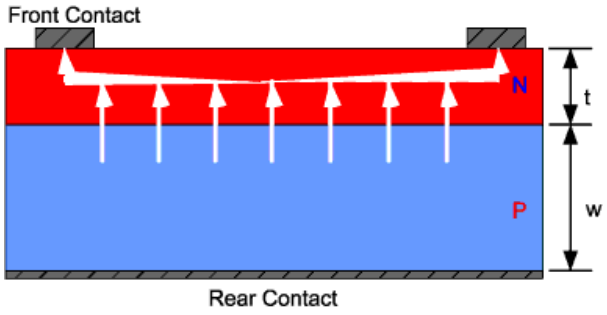

Figure 1 Resistance faced by charged carriers in solar cell

2.1.3 Finger Resistance

For higher conductivity and better charge collection from the top surface of a cell, it has a series of uniformly spaced fingers. Ideally, tapering the fingers is expected to reduce losses, however, technological limitations make it hard to achieve such structure so fingers usually have uniform width [3].

2.2 Metal Grid Pattern

While designing the top contact for a solar cell, reducing finger and busbar resistance is a key factor that needs consideration, however, other losses associated with top contact also bear crucial significance. These include resistive losses at interface of contact and emitter as well as optical and shading losses of the top contact. The pitch, aspect ratio of the fingers and busbars and resistivity of the material used for depositing the grid are critical features that determine the magnitude of these losses in the top contact.

2.2.1 Impact of Finger Spacing on Emitter Resistance

Power loss in the emitter is dependent upon the space between individual fingers that electrons must travel to get to them. Hence, tightly packed fingers are can collect charge more effectively reducing emitter resistance [4].

2.2.2 Grid Resistance

Grid resistance depends upon the grid feature design, resistivity of material used to make it and aspect ratio of fingers. The use of a highly conductive material to form high aspect ratio contacts is desirable but hard to attain using conventional technology.

2.2.3 Shading Losses

Shading losses occur due to the shadow caused by grid features, reducing the amount of light entering the solar cell [5]. The minimum line width is a significant practical limitation associated with a particular contact grid technology. These losses can be determined by measuring the percentage of cell top surface covered by metallic contacts to calculate the total transparent area. Transparency depends upon the aspect ratio of the fingers.

2.2.4 Design Rules

There exist a multitude of front metal grid design schemes, however, most of the design in use are kept highly symmetrical and relatively simple for practical reasons. A few key design rules are as follows [6].

- Busbar width is optimum, W_B, when the resistive loss in busbar equal the shading loss.
- Tapering the fingers leads to lower losses than uniform width
- Losses can be reduced by designing a metal grid with smaller finger width, and shorter pitch.

2.3 Transparent electrodes for organic printed solar cells

Transparent conductive oxides (TCOs) are the most widely used material for depositing transparent electrodes as the rear and top contacts. Indium tin oxide (ITO), fluorine doped tin oxide (FTO) and doped zinc oxide (ZnO) etc are the most commonly used TCOs and they are deposited using vacuum based thin film technology such as plasma enhanced chemical vapor deposition (PECVD), pulsed laser deposition, DC/RF sputtering or sol gel method. Once deposited, they give sheet resistance of the order of 10 ohm/square and can perform well without additional metal grid.

2.3.1 Tin doped indium oxide (ITO)

Tin doped Indium Oxide (ITO) is a binary composite, consisting of 90% Indium oxide doped with 10% Tin oxide. It has multiple applications due to its high infrared reflectivity, fair electrical conductivity and high transmittance in the visible region of the spectrum. The optical transparency of ITO is around 90%. TCOs are used in photovoltaic devices, waveguide electron devices, LCDs and light emitting diodes [7].

Properties of the ITO depend majorly on how it has been deposited and specific control of the process parameters. Despite many advantages, ITO is mechanically fragile as it is quite crystalline, exhibiting high brittleness and can be damaged easily. The major obstacle to their widespread application, however, is that they require vacuum-based thin film technology for deposition, which adds to their cost. One kilogram of ITO costs approximately 1000 USD because Indium is a rare metal.

2.3.2 Reducing ITO top electrode thickness to reduce reflection losses

Minimizing reflection and parasitic absorption losses is crucial to attaining high performance efficiencies in third generation solution processed solar cells such as perovskites (PVKs), Lead Lanthanum Zirconium Titanate (PLZT) [8] and Lead Zirconium Titanate (PZT) solar cells [9] that employ transparent conductive oxides (TCOs) as the top surface contacts. This is also necessary to achieve high matched current densities in the champion tandem devices, solar cells where each layer is evaluated to ensure that it offers minimal loss to overall device performance. The previous record efficiency tandem solar cell device [10] was unable to capture almost 5 mA cm^{-2} across the spectrum due to reflection loss. Characterization of the optical constants for each material in the device stack coupled with optical simulations of the PVK/Si tandem devices with varying TCO thickness indicated that reducing the TCO thickness from 150nm to 60nm proves beneficial, as it blue-shifts the maximum reflection from 550nm to 400nm. This reduces the reflection loss attributed to the TCO, as there is relatively less absorption in this region of the solar spectrum corresponding to the band gap of the material [11]. This reduction in front TCO layer thickness also reduces parasitic absorption, which is around 2.38 mA/cm^{-2} for 500nm thick FTO layer in perovskite solar cells [12]. [11]

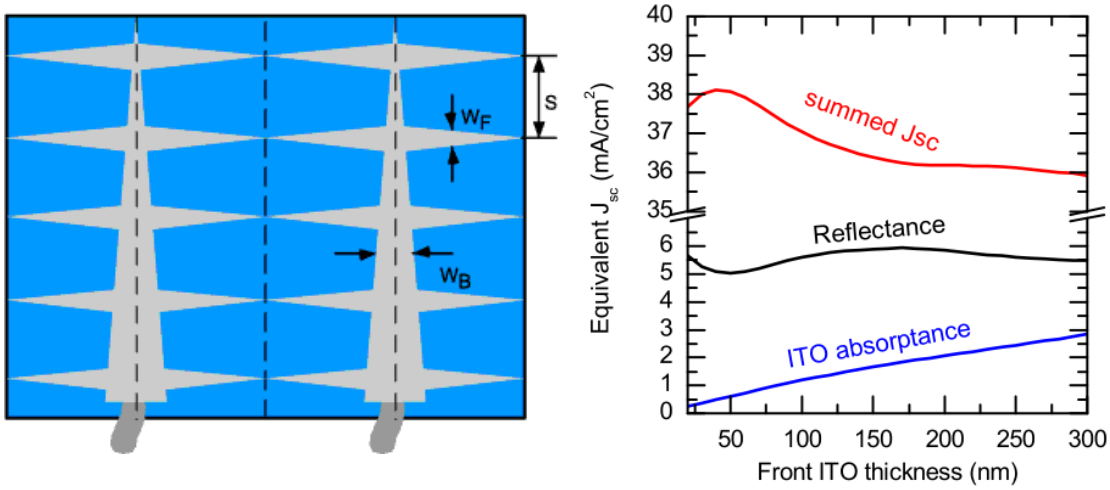

Figure 2 a) Schematic of a top contact design showing busbars and fingers b) Effect of reducing TCO thickness on J_{sc}

Figure 2 b) shows how decreasing the ITO thickness from 150 nm to 50–60 nm leads to an increase in the summed J_{sc} of approximately 2 mA/cm^2 in the Perovskite and silicon absorber material. Reducing the ITO thickness, however, beyond a certain limit is known to increase the resistive losses because the sheet resistance varies with thickness. Upon reducing the thickness of the ITO by 2.5 times, the sheet resistance increases from 33.3 to 83.3 Ω/sq and the fill factor (FF) decreases more than 2% [11]. To reduce the optical and parasitic absorption losses of ITO, thin fingers of a conductive paste or ink can be deposited on top of a thinner layer of ITO, which would simultaneously reduce the lateral distance that charge carriers would need to travel, along with the shadowing losses. Such fingers were deposited on top of a thin ITO layer, using a shadow mask with a two finger pattern inscribed on it. The length of these fingers was approximately two thirds of that of the device. Thinner fingers would reduce J_{sc} losses by reducing the amount of shading. Multiple techniques like inkjet printing [13], microchannel contacting [6], gravure printing [4],[2],metal wrap through [14], screen printing [15], aerosol fine line printing [11], and copper plating [16] have been used for trying to deposit thinner fingers. Some of these techniques are being used on trial project lines, but most of them are based on modest aspect ratios and their use is limited for a specific type of surface.

2.4 Metal grid for third generation solar cells

An effective metal contact grid must cater a number of issues that include line resistance, contact shading, contact resistance, transparency, reflective losses, cost and

technological limitations. The minimum finger width that can be successfully achieved is 40 μm and the best aspect ratio achieved is 0.5 [11]. The paste that are commonly used to make low resistance contacts require high temperatures for curing i.e. >200 ºC. Owing to these limitations, a lot of research has been done in this area, for developing the optimum grid design having a high aspect ratio, narrow fingers and low interfacial resistance using high conductivity material that cures at lower temperatures.

2.4.1 Effectively Transparent Contacts (ETCs)

One of the most interesting approaches to developing a high aspect ratio and low finger width metal grid is via microchannel contacting. In this approach, a polymer mold inscribed with microchannels is used in which a conductive fluid is passed [6]. It is then cured at a certain temperature and the mold is removed, leaving behind a metal grid of microscale fingers that run over the charge transport or ITO layer. In one such method, two photon lithography was used to fabricate a silicon master mold engraved with a microchannel grid pattern [17]. This master mold was used to develop a secondary mold from polydimethylsiloxane (PDMS) that was cured at 90ºC. The developed PDMS stamp was inscribed with a grid of many fingers that ran parallel to each other across the length of the mold, with the pitch of this grid 40 μm, width of 2.5 μm and height of 7 μm. Results from simulations indicate that reducing ITO thickness in perovskite solar cells can improve the J_{sc} by more than 1 mA/cm^2. None-the-less, to reduce lateral charge transport losses, an additional metal finger grid is required. Effectively transparent contacts (ETCs) are triangular cross-section silver fingers of microscale that function to redirect the incoming solar radiation to the absorber layer of the solar cell. These microscale contacts are placed so closely together because of the small diffusion lengths in perovskites. If spaced densely, these ETCs exhibit high lateral conductivity [18] and have the potential to reduce TCO layer thickness, or replace it altogether [1] increasing the short circuit current density and mitigating the losses due to parasitic absorption and reflection.

2.4.2 Light trapping using Effectively transparent contacts (ETCs)

The triangular cross-section ETCs of microscale, successfully redirect incident light towards the absorber layer of the solar cell, mitigating shading losses. Moreover, their tight packing leads to lower energy photons being trapped, causing an increase in J_{sc}. This tight spacing also makes it possible to use a single busbar instead of three. The optimum grid design would consist of just one busbar with a 20% area coverage by

ETC on the front surface and around 20-30% of the cell area coverage towards the rear end, according to the intensity of illumination. Following this configuration, an increase of approximately 4.4-4.6% is expected to be seen in the J_{sc} with a reduction in the amount of ink used.

2.4.3 Effectively transparent contacts (ETCs) as superstrates for perovskites

The use of ETCs for perovskite solar cell by incorporating them into superstrates results in high conductivities (sheet resistivities lower that 5 Ω/sq) and transparency approaching 99%. Such superstrates have been fabricated with a confirmed effective transparency of >99%. Optical simulations were carried out for measuring the effect of total internal reflection due to the triangular cross-section of the grid fingers and the results indicate that the absorption in the absorber layer can even exceed that of cells without metal grids because of improved light trapping [19]. Such superstrates are compatible with most thin film and tandem solar cell technologies [18], however, ETCs cannot be used on textured surfaces.

2.5 Polydimethylsiloxane (PDMS)

Polydimethylsiloxane (PDMS) belongs to the class of polymers known as organosilicon polymers, more commonly referred to as silicones. PDMS is the most widely used polymer and ranges in application from silly putty to cosmetic and medicine. It is a transparent polymer having a glass like appearance upon curing, but is highly flexible, depending on its thickness. It is best known for its use in microfluidic devices and can be used easily to make a microchannel mold from a master mold, curing at temperatures around 150 ºC.

2.5.1 Plasma surface cleaning for improved bonding

Plasma treatment using Air/Ar plasma is required to improve adhesion of PDMS to the substrate. This treatment works to remove certain impurities on the surface of both the PDMS and solar cell substrate, getting rid of hydrocarbons and replacing them with silanol groups on the polymer and OH groups on the substrate [20]. In case of a glass substrate, this treatment results in the formation of Si – O – Si covalent bonds upon adhesion. Another purpose of this treatment is to increase the hydrophilicity or wettability of both surfaces, which is a crucial factor while using polar liquids.

2.5.2 Capillary action

Capillary action occurs as a result of the forces of cohesion and adhesion. Cohesive forces in the water molecules give them the tendency to stay together and adhesive forces make it stick to other substances (like glass). Adhesion of water molecules with the walls of a vessel create an upward force that acts on it at the edges, resulting in a meniscus which curls upward. The surface tension holds the surface in place and the water level does not drop. Capillary action occurs only when the forces against the wall are stronger than the forces of cohesion between the molecules of the liquid. The distance travelled by the liquid via capillary action in a uniform groove is limited by surface tension and gravity [21].

2.6 Reactive Silver Ink

In the rapidly growing field of printed electronics, conductive inks have a special significance in that they are extremely flexible in their applications. However, some methods face technical difficulties due to the presence of particles in these inks, e.g. when using ink jet printing, a particle free ink is required which would not clog the printer nozzle. There are certain requirements that a good, particle free ink must meet i.e. optimum viscosity, formation of non-porous uniform films with high chemical sintering, in-situ reduction, jetting and storage stability, high conductivity and good adhesion. A Recipe based on a modified Tollen's reagent was developed by Walker et. al. [22]. The basic components of this Reactive Silver Ink are a Silver salt, a complexing agent (usually amine based) and a reducing agent (short-chain carboxylic acid). Upon evaporation of the solvent, reduced silver is left behind which is used to form the required conductive structures. This ink is simple to synthesize and high yielding, no residual educing agent is left behind and the weight percentage of silver after annealing the ink at 90°C is 22% [22].

2.7 Perovskite Solar Cells (PVKs)

This class of solar cells belongs to the third-generation solar cell technology and resemble closely with the Dye Sensitized Solar Cells (DSSCs) with a few differences in the device architecture. They have a hybrid organic-inorganic light absorbing layer instead of a liquid dye. The basic types of perovskites devices include the planner heterojunction and Meso-super structured PSCs based on whether they possess a

mesoporous TiO_2 electron transport layer. General structure of the perovskites is given below.

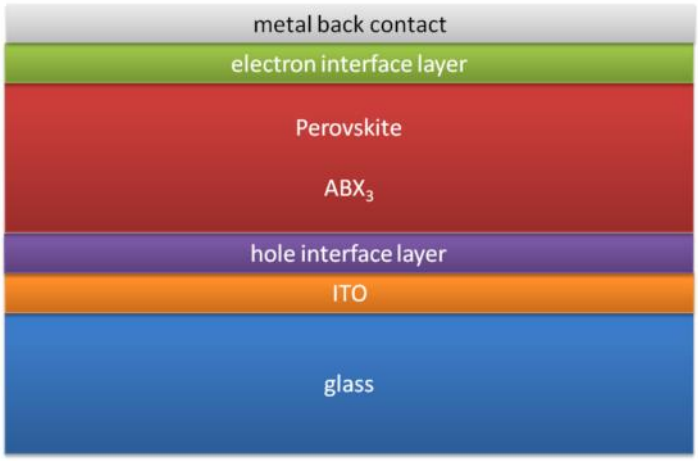

Figure 3. General structure of perovskite solar cell in substrate configuration

1. **Bottom Glass substrate**

A bare glass slide acts as the substrate upon which the remaining layers are deposited. In substrate configuration, this glass slide is the bottom most layer, whereas in superstrate configuration, it acts as the top most layer and light is passed through it on to the other layers.

2. **Transparent conductive oxide (TCO)**

The glass substrate is coated with an optimum thickness Tin doped Indium Oxide (ITO) layer to facilitate lateral transport in the device. Another layer of TCO is deposited above the ETL as the top metal contact in many cases.

3. **Hole transport layer (HTL)**

This layer facilitates the hole transport and is usually made of an organic or inorganic material like Spiro-MeOTAD, PTAA, PEDOT:PSS, NiO or CuSCN.

4. **Perovskite**

This layer is composed of the perovskite material (ABX3) and functions as the absorber material. Electron and hole pairs are produced when light hits this layer, from where they are transported to the particular charge transport layers.

5. **Electron transport layer (ETL)**

This layer captures the electrons so that they do not undergo recombination again and transports them to the metal contact.

6. **Metal grid**

The purpose of this grid is effective charge collection. The electrons produced at the absorber are passed on to the ETL form where they must travel to the metal grid that transports them to the external circuit.

2.7.1 Low temperature curing contacts for Perovskites

Perovskite solar cells are of great interest due to the huge amount of flexibility in their compositional structure and ease of manufacture. However, a number of factors inhibit their performance and decrease their durability many times, as compared to conventional semiconducting material [23]. Even now, with many improvements in their performance parameters, their average lifetimes are only a few thousand hours under standard testing conditions. Perovskite absorber material is sensitive to high levels of moisture in the surrounding, high temperatures, many solvents that readily degrade the absorber layer (protic and aprotic), rendering it useless. One of the major issues that faces these cells when it comes to depositing suitable contacts, is the high temperature required for firing the conducting material (paste or ink) used to fabricate these contacts, which may be as high as 850 °C depending upon the type of paste used. In particular, methyl ammonium based perovskites show lower tolerance towards higher temperatures (becoming unstable at 55 °C) , whereas formamidinium based perovskites can withstand temperatures > 150 °C. incorporation of Cesium (Cs) into the formamidinium based PVK absorber helps to improve thermal stability to some extent [24]. In addition to this, certain charge transport materials, such as PTAA and NiOx are also sensitive to high temperatures.

2.8 Summary

This chapter overviews all the losses incurred by the metal grid using conventional methods and the need for a metal grid design that is developed based on a trade-off between these losses. Transparent conductive oxides are effective, exhibit good conductivity and are used for third generation solar cells, but the charge collection in these cells can be further enhanced by using an ITO layer of reduced thickness coupled with an effectively transparent metal contact grid. Many solar cell technologies involve the use of materials that are sensitive to relatively high temperatures, such as the absorber layer in perovskite solar cells, charge transport layers like PTAA and NiO_x cannot withstand higher temperatures and amorphous silicon in silicon heterojunction solar cells is only stable below 200°C. Thus, effectively transparent microchannel contacts, developed using a low temperature reactive silver ink can be used to improve charge collection by the sputter deposited ITO layer.

References

[1] R. Saive *et al.*, “Sustainable Energy & Fuels Silicon heterojunction solar cells with e ff ectively transparent front contacts,” *Sustain. Energy Fuels*, vol. 00, pp. 1–6, 2017.

[2] R. Saive *et al.*, “Effectively Transparent Front Contacts for Optoelectronic Devices Supplemental : Effectively transparent front contacts for optoelectronic devices,” 2016.

[3] Y. K. Fang *et al.*, “Contact Resistance : Its Measurement and Relative Importance to Power Loss in a Solar Cell,” no. 5, 1984.

[4] R. Saive *et al.*, “Effectively Transparent Front Contacts for Optoelectronic Devices,” pp. 1470–1474, 2016.

[5] A. M. A.M. Jeffries, “Low temperature DoD RSI for front grid metallization [Autosaved].” .

[6] J. Bullock *et al.*, “Microchannel contacting of crystalline silicon solar cells,” pp. 1–8, 2017.

[7] M. A. Aouaj, R. Diaz, A. Belayachi, F. Rueda, and M. Abd-Lefdil, “Comparative study of ITO and FTO thin films grown by spray pyrolysis,” *Mater. Res. Bull.*, vol. 44, no. 7, pp. 1458–1461, 2009.

[8] M. Hordagoda, “Growth , characterization , and function of ferroelectric , ferromagnetic thin films and their heterostructures,” no. November, 2017.

[9] Y. H. Paik, “Novel Photovoltaic Devices using Ferroelectric Material and Colloidal Quantum Dots,” 2017.

[10] K. A. Bush *et al.*, “23.6%-Efficient Monolithic Perovskite/Silicon Tandem Solar Cells With Improved Stability,” *Nat. Energy*, vol. 2, no. 4, pp. 1–7, 2017.

[11] K. A. Bush *et al.*, “Minimizing Current and Voltage Losses to Reach 25% Efficient Monolithic Two-Terminal Perovskite–Silicon Tandem Solar Cells,” *ACS Energy Lett.*, pp. 2173–2180, 2018.

[12] Y. Da, Y. Xuan, and Q. Li, “Quantifying energy losses in planar perovskite solar cells,” *Sol. Energy Mater. Sol. Cells*, vol. 174, no. January, pp. 206–213, 2018.

[13] A. M. Jeffries, A. Mamidanna, L. Ding, O. J. Hildreth, and M. I. Bertoni, “Low-Temperature Drop-on-Demand Reactive Silver Inks for Solar Cell Front-Grid Metallization,” vol. 7, no. 1, pp. 37–43, 2017.

[14] I. J. Bennett, “Cost , efficiency and material optimisation of back-contact cell and module design,” *Energy Procedia*, vol. 55, pp. 374–379, 2014.

[15] D. Inns, “Understanding metal induced recombination losses in silicon solar cells with screen printed silver contacts,” *Energy Procedia*, vol. 98, pp. 23–29, 2016.

[16] J. J. P. Valeton *et al.*, “Room temperature preparation of conductive silver features using spin-coating and inkjet printing,” *J. Mater. Chem.*, vol. 20, no. 3, pp. 543–546, 2010.

[17] R. Saive, C. R. Bukowsky, and H. A. Atwater, “Three-dimensional nanoimprint lithography using two-photon lithography master samples,” pp. 1–4, 2017.

[18] R. Saive, S. Coplin, H. L. Kim, C. H. Van De Stadt, D. Michael, and H. A. Atwater, “Transparent , Conductive and Lightweight Superstrates for Perovskite Solar Cells and Modules,” pp. 1–5.

[19] P. Jahelka, R. Saive, and H. Atwater, “Total Internal Reflection for Effectively Transparent Solar Cell Contacts,” pp. 1–14, 2016.

[20] A. Note, “Plasma Treated PDMS for improved bonding performance of microfluidic devices Plasma Treated PDMS for improved bonding performance of microfluidic devices,” vol. 44, no. 0, pp. 0–5, 1925.

[21] H. (The U. water science school) Perlman, “USGS science for a changing world.” [Online]. Available: https://water.usgs.gov/edu/capillaryaction.html.

[22] S. B. Walker and J. A. Lewis, “Reactive silver inks for patterning high-conductivity features at mild temperatures,” *J. Am. Chem. Soc.*, vol. 134, no. 3, pp. 1419–1421, 2012.

[23] J. Bisquert, Y. Qi, T. Ma, and Y. Yan, “Advances and Obstacles on Perovskite Solar Cell Research from Material Properties to Photovoltaic Function,” *ACS Energy Lett.*, vol. 2, no. 2, pp. 520–523, 2017.

[24] Y. Yu, C. Wang, C. R. Grice, N. Shrestha, J. Chen, and D. Zhao, “Improving the Performance of Formamidinium and Cesium Lead Triiodide Perovskite Solar Cells using Lead Thiocyanate Additives,” pp. 1–11, 2016.

Chapter 3: Experimental Techniques and Characterization Tools

3.1 Two photon lithography for master mold

This is a technique that belongs to the direct laser writing family. A lot of UV photosensitive materials can polymerize by simultaneously absorbing two N-IR photons but the likelihood of this non-linear optical process to occur increases by focusing an ultrashort pulse laser on to a compact given area which is determined by the laser spot and power. It is possible to polymerize the photoresist using an ultrashort pulse laser that can pattern 3-D structures having feature in the size range of 100 nm. For this reason, two-photon lithography also known as nano 3-D printing. Just as any other 3-D printing technique requires drafting of the the desired shape using a computer assisted design (CAD) program, two photon lithography also needs developing of the design beforehand. Changes in the shape can be made easily by making a few alterations in the process parameters. Nano 3-D printing has led to many scientific breakthroughs from nano and micro optics to nano and micro mechanics [1].

3.2 Plasma surface cleaning

Plasma is the state of the matter in which gas molecules, ions and free electrons coexist. The plasma surface cleaner achieves the formation of plasma via high frequency electromagnetic field. Gas molecules in this mixture react with the surrounding materials. The effect of this plasma reacting with the exposed substrate is that it creates dangling bonds, making the substrate highly reactive towards certain materials [2]. This works to not only clean the substrate, freeing it from carbon-based impurities and debris, but also increases the adhesion of substrate to many materials. The strength of the plasma and nature of the gases used depends upon the specific task it is intended for. Adhesion as strong as 75psi (0.5 MPa) can be reached between the glass and PDMS [3].

3.3 Spin Coating

This is a relatively simple yet effective technique for thin film deposition, in which a solution (organic, inorganic or hybrid) is dropped onto the substrate at a steady rotation rate. Once the process is optimized, it can be used to produce high quality films of the desired material dissolved in a suitable solvent . The deposited film ranges in thickness from a few nm to many um. The substrate is placed on the spin coater which is held in place

by the vacuum generated by rotary pump. The speed of rotation can be adjusted from anywhere between 100-10000 rpm and time duration (in seconds) is adjusted by built-in controlling speed and time functions. The solution is injected on to the substrate through a syringe or pipette. The film thickness is inversely proportional to the speed of rotation and is dependent upon factors such as solvent evaporation rate, solution concentration, viscosity and temperature of the substrate [4]. Only one substrate can be coated at a time, so the process is a little slow as compared to roll to roll process and quick drying of films can lead to highly porous and poorly chemically sintered layers. A large fraction of material goes to waste as it flies off during spinning of the substrate.

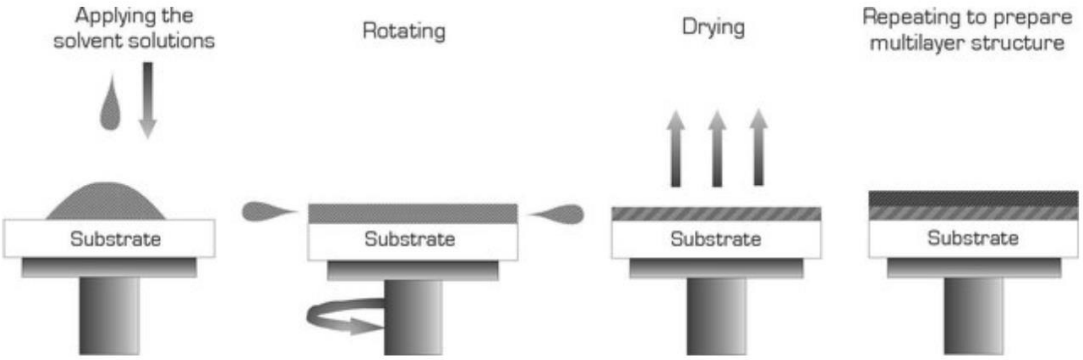

Figure 4. Steps involved in spin coating

Applications

It is used to coat substrates with everything from insulators, photoresists, organic semiconductors, nanomaterials, metal, synthetic metals, transparent conductive oxides and many other materials.

3.4 RF sputtering

Radio Frequency sputtering uses an alternating electric potential in a vacuum environment to avoid the build up of charge on certain sputter targets, which can result in arcing into the plasma over time, leading to droplet spewing that causes quality control issues in the film. It is a much more effective technique, as compared to DC sputtering and gives high quality films at low temperature substrates. RF plasma tends to diffuse uniformly throughout the chamber whereas DC plasma is concentrated around the target material or cathode. Lower pressure is required to sustain the plasma and this technique is suitable for substrates that can not withstand higher temperatures but since RF sputtering uses radio waves instead of DC current, the rate of deposition is much slower and much higher voltages are required for this system (approximately 1012).it is possible to sputter an electrically insulating target using RF sputtering.

Working principle

The RF-sputtering device is comprised of a cathode, known as the target and an anode which is placed in series along with a blocking capacitor. This whole assembly is part of an impedance matching network. A high voltage RF source is used to supply power and is commonly fixed at 13.56 MHz.

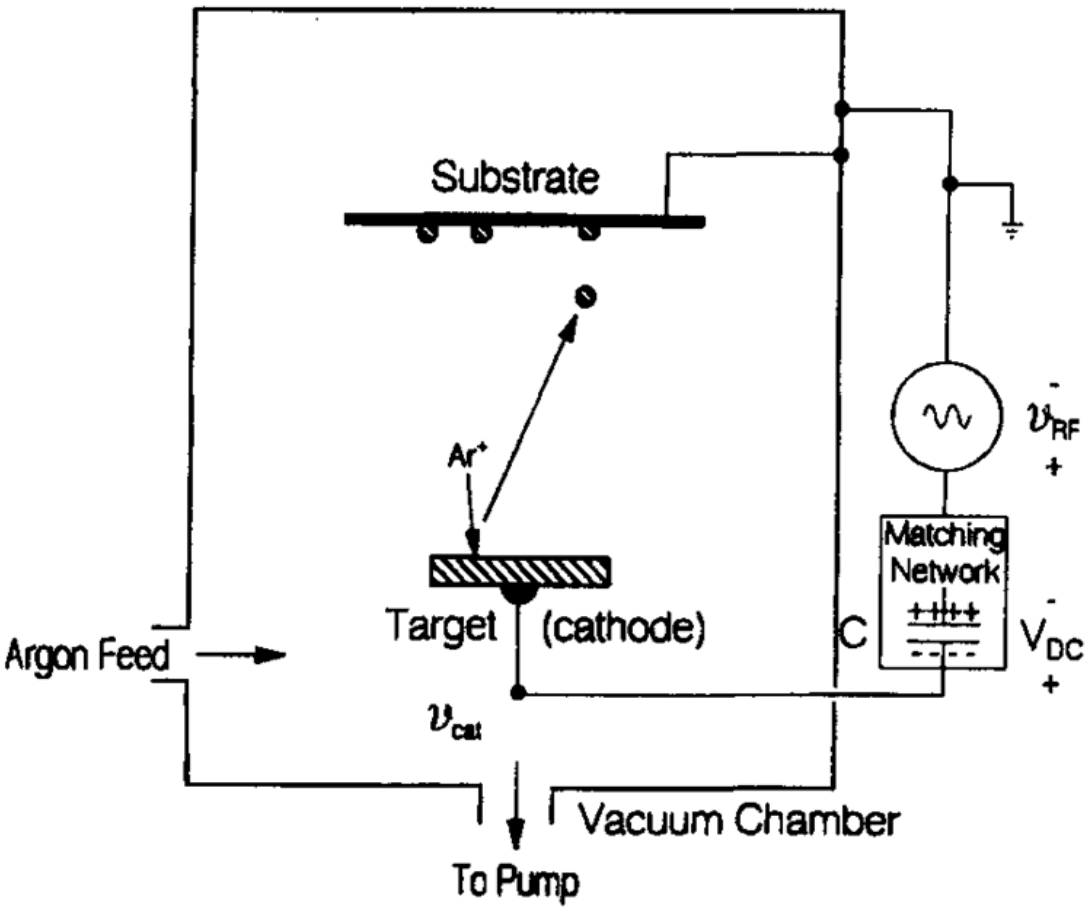

Figure 5. Schematic diagram of RF sputter process

3.5 Etching

There are two methods for etching a surface i.e. wet chemical etching and dry etching. In wet chemical etching, the substrate is dissolved in a chemical solution and the desired material is removed as the result of a chemical reaction. For example, single crystal silicon undergoes anisotropic etching when treated with potassium hydroxide (KOH), resulting in a pyramidal textured surface of the silicon wafer. Dry etching consists of methods such as reactive ion etching (RIE), sputter etching, vapor phase etching and other physical means such as scraping with a scalpel or blade to physically remove the material [5].

3.6 Ultraviolet–visible spectroscopy

The amount of light transmitted by contacts is a measure of its transparency. Conventionally, the thickness of ITO deposited on thin film solar cells is from 50-200 nm and measurement of transmittance shows that it allows greater than 90% of the incident light to pass through. UV-Vis spectroscopy is a technique which measures absorption, transmittance and reflection in the ultraviolet (190 nm-400 nm) and visible (400 nm- 700nm) regions. It also gives information about the organic molecules and helps to determine the presence of impurities, heteroatoms, saturation or unsaturation in the material. UV-Vis spectroscopy is majorly used for determining the compounds present within a sample by comparing the spectrum obtained with those of known compounds.

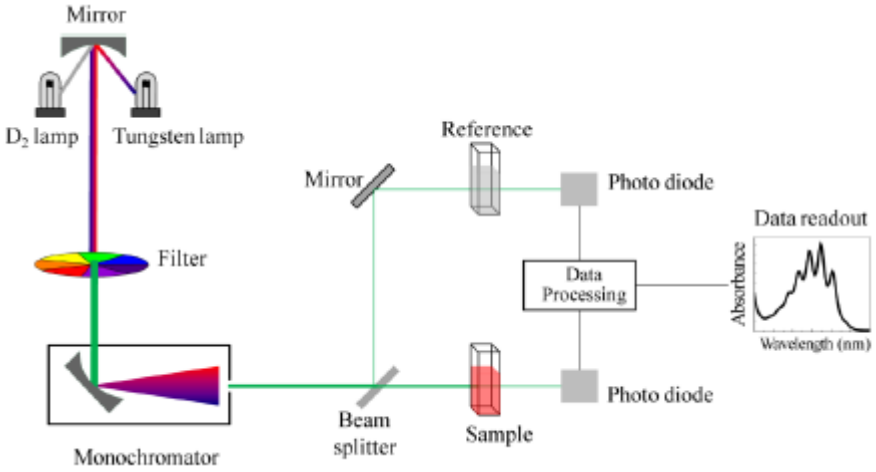

Figure 6. Working principle of UV-Vis spectroscopy

Working principle

The sample is placed under the lamp and light passes through it, exciting the electrons to anti-bonding orbitals. Lower the energy difference between HOMO and LUMO of a material, the easier it is to excite them using longer wavelength radiation. This electronic transition between the bonding to anti-bonding is denoted by σ - σ*. A graph is obtained as a result of measuring the interaction of radiation with the sample molecules such that the transmittance/absorbance is given on the y-axis, whereas the effective wavelength is plotted along the x-axis.

3.7 Thermogravimetric analysis

Thermogravimetry is a thermal analysis technique which studies the changes in physical and chemical properties of a substance as a function of temperature (in scanning mode) or time (in isothermal mode). TGA measures the changes in mass of the sample that occur due to various thermal events like adsorption, desorption, vaporization, sublimation, decomposition, reduction, oxidation. It is used for the analysis of volatile substances, gaseous products and polymers.

3.8 Optical microscope

This technique is used for many different purposes in academia and industry. A simple microscope uses visible light and can magnifies the any material surface for analysis. For producing a magnified image of a sample, there are three basic steps involved i.e. 1) obtaining a clear, sharp image 2) changing the magnification 3) adjusting focus. When used for these purposes, the optical system is called the observation optical system. Whereas, when it is used for the purpose of supplying, collecting light at various intensities, it is called an illumination optical system.

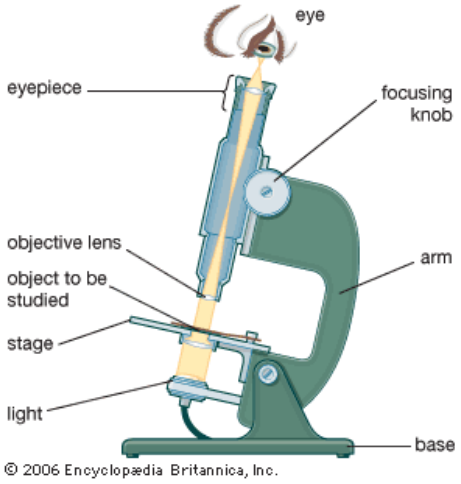

Figure 7. Components of an Optical Microscope

Working principle

A compound microscope consists of two or more lenses that generate a magnified image of the specimen which is placed on a glass slide at the base. The microscope is fixed on a stand and light from a bright lamp or sunlight shines through it from the bottom. These rays of light fall on to an angled mirror and are reflected onto the specimen. The mirror is adjustable and can be pivoted such that it catches maximum light and brightens the image [6]. The light passes through a hole in the stage, which an adjustable horizontal platform. The stage can move up and down upon turning a thumb wheel on the side of the device. Using this knob, the stage can be raised or lowered, bringing the lenses closer to or further away from the specimen under examination and adjusting the focus. The specimen must be such that it allows light to pass through it to get an image.

3.9 Scanning Electron Microscopy (SEM)

The scanning electron microscope (SEM) directs a focused beam of electrons to produce a variety of signals at the substrate surface. These signals give information about the substrate morphology (texture), crystal structure and chemical composition. It generates a 2-dimensional image

that shows the variations in these properties. The wavelength of electrons is around 1000 times shorter than visible light, meaning that SEM can magnify and resolve images much better than an optical microscope. In the scanning mode, areas ranging from almost 1 cm to 5 um in width can be imaged, magnification ranges from 20X to 30,000X and a spatial resolution of 50 to 100 nm [7]. Using the SEM, it is possible to perform an analysis of selected sites on the sample surface. Moreover, an additional feature, known as Energy Dispersive X-ray Spectroscopy (EDS) is used to determine the chemical compositions of the sample. Information regarding the crystalline structure orientations of the crystal can be obtained using Electron Backscatter Diffraction (EBSD) .

Working principle

The electron beam is generated thermionically by using electron gun fixed on a tungsten filament cathode. The tungsten metal has the highest melting point and lowest vapor pressure so it can be used for electron beam generation via heating thermionic electron guns. The focusing and controlling of electron beam is achieved by using condenser lenses of diameter range ~4–50 Å and deflection coils respectively. The schematic diagram of SEM is shown in Figure 3.10 which shows the complete flow of process from the start i.e. generation of electron beam to end i.e. the beam strikes the sample. Finally, the generated signals i.e. secondary electrons are analyzed with the help of detector and the output is displayed [12].

When the electron beam hits the sample surface different types of signals generates carrying information about film or surface morphology. These signals include X-rays, secondary electrons and back scattered electrons. Finally, these signals can be detected by specific detectors and the chemical composition of material is analyzed by back scattered electrons while secondary electrons give surface morphology. High vacuum and non-conductive surface of sample are the conditions of using this technique [13].

3.10 Atomic Force Microscopy (AFM)

AFM is a surface imaging technique that provides a 3D profile of the substrate surface at nanoscale. This is achieved by measuring the force between a surface and sharp probe (<10 nm). This probe is supported on a flexible cantilever and the AFM tip softly grazes the surface , recording the variations in force upon contact of the probe with the surface [8].

Van der Waals (VdW) interactions are the most dominant type of short-range interactions between the probe and substrate, however, long-range interactions become significant at some distance from the surface. Upon contact with the sample substrate, the probe experiences repulsive *Van der Waals* forces (in contact mode), which causes the tip to deflect. When the tip moves further away, attractive Van der Waals forces become dominant (in non-contact mode).

Imaging modes in Atomic force microscopy

1. **Contact Mode AFM**

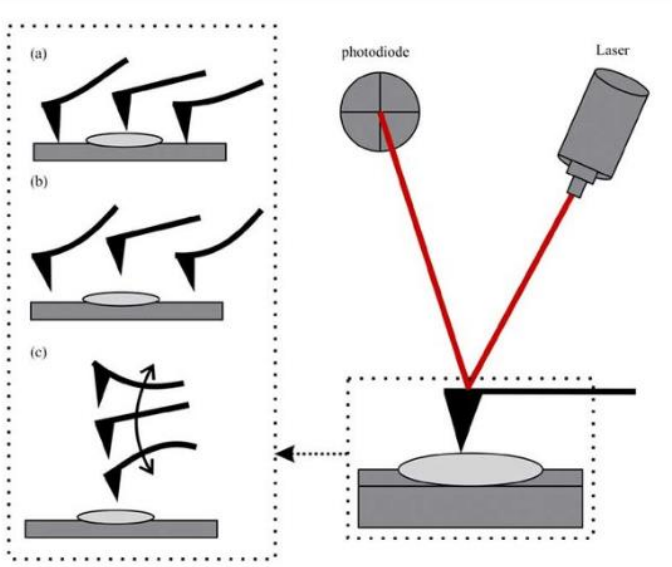

Figure 8. . Imaging modes in AFM a) contact mode b) non-contact mode c) Tapping mode

This is based on the repulsive Van der Waals forces. Probe-surface separation in this mode is < 0.5 nm. The cantilever bends when its spring constant is less than surface. The force on the tip is repulsive. The force between the surface and probe remains constant by maintaining a constant cantilever deflection and the surface image is obtained.

2. **Intermittent Mode (Tapping)**
   This is similar to contact mode, but the cantilever is made to oscillate at its resonant frequency. Probe-surface separation ranges from 0.5-2 nm in this mode. The probe gently 'taps' the sample surface during scanning, making contact with the surface at the bottom of its swing. A higher resolution is obtained using this mode by maintaining uniform oscillation amplitude which ensures a constant tip-sample interaction.
3. **Non-contact Mode**
   This mode involves attractive Van der Waal's forces and the probe does not touch the sample surface, but merely oscillates above a layer of adsorbed fluid on the surface. The surface topography is measured using a feedback loop for monitoring changes in the amplitude because of the

attractive Van der Waal's forces. Probe-surface separation in this mode is 0.1-10 nm.

3.11 Hall effect measurement

The Hall effect can be observed when an electrical current is generated perpendicular to an externally applied magnetic field and a current that flows across the length of the sample. This in turn, produces a transverse voltage that also acts perpendicular to both current and magnetic field. This effect is based on the principle of Lorentz force, i.e. the force on a point charge due to electromagnetic fields [9]. Direction of the flow of current can be determined using the "right hand rule". The Hall voltage is measured to determine the nature of the semiconducting material (n-type or p-type) the carrier mobility and the free carrier density. The free carrier density, along with the charge carrier mobility can be measured as a function of temperature by repeating measurements at varying temperatures.

Consider a conducting slab with length L in the x direction, width w in the y direction and thickness t in the z direction [10]. Let, the conductor has charge carriers of charge q, a charge carrier density n and charge carrier drift velocity vx. The current Ix through this slab flows along the positive x-axis. The current Ix is the current density Jx times the cross-sectional area of the conductor wt. wt. The current density Jx is the drift velocity vx times the charge density nq. Hence,

$$\mathbf{I_x = J_x wt = nqv_x wt \quad (1)}$$

The current I_x is generated due to application of an electric field along the conductor length when current is directly proportional to the applied electric field, the material is said to exhibit ohmic behavior.

$$\mathbf{J_x = \sigma E_x \quad (2)}$$

where σ is the conductivity of the material in the conductor.

Since the applied magnetic field is perpendicular to the plane of the slab, the charge carriers experience a Lorentz force $q\mathbf{v} \times \mathbf{B}$ which causes them to deflect to one side of the slab, producing a transverse electric field Ey that counterbalances the magnetic field. When steady state is approached, there is no net flow of charge along the y direction because electrical and magnetic forces on charge carriers in that direction must be balanced. Assuming these conditions, it is easy to show that

$$\mathbf{E_y = v_x B_z \quad (3)}$$

where E_y is the electric field/Hall field, in the y direction and B_z the magnetic field in the z direction.

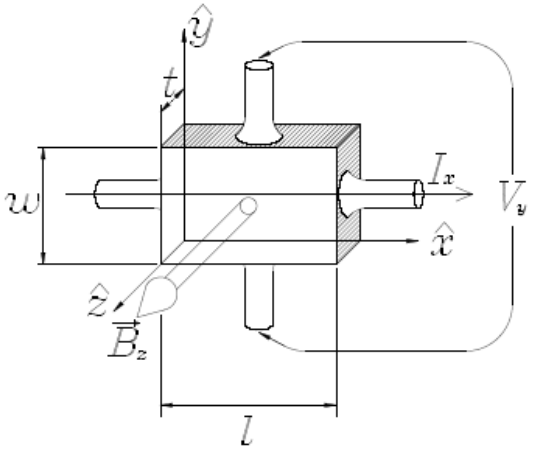

Figure 9. Geometry of fields and sample in Hall effect experiment

3.12 IV-curve Measurement

The I-V curve is a graph of all possible available combinations of voltage and current operated under constant conditions and give the characteristic electrical properties of a solar cell depending upon the active electrode region that enhances charge transport, exciton dissociation and carrier injection. These properties a usually measured using a Keithley source meter under illuminated and dark conditions. Generally, the I-V curve has a characteristic shape point, the behavior is similar however, when it is to the right of the MPP, there is an immediate decline in power output because of sealed charges within the solar cell that do not flow out. These charges are a result of increased voltage output [11]. IV-curve gives the short circuit current (I_{sc}), open circuit voltage (V_{oc}) and Fill Factor (FF) for the device under consideration and this information can be used to calculate the performance efficiency of the device.

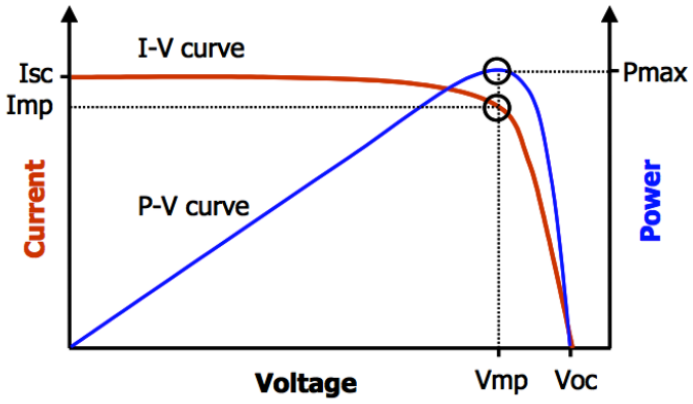

Figure 10 IV-curve measurement using one sun solar simulator

The fill factor one of the most important performance indicator that illustrates the ratio of the two areas that are indicated by the I-V curve. When comparing different PV modules with the samIsc and Voc, the highest fill factor will thus yield more power. Theoretically the upper right corner of each building sblock represents the MPP.

3.13 Summary

This chapter describes the experimental methodology, material synthesis and working principle of various characterization techniques that were used. Spin coating is an easy and inexpensive technique for the formation of a uniform thin film through solution processing. The films formed using this technique were characterized for morphological, optical and electrical properties using optical microscope and Hall effect measurements. Morphological and structural characteristics of the sample can be observed effectively using optical microscope, SEM and atomic force microscopy (AFM) while Hall effect measurement and IV-measurements give information about the electrical characteristics of a sample. UV-Vis analysis of the samples gives information about their optical properties such as absorbance, transmittance and reflectance e.t.c.

References

[1] R. Saive, C. R. Bukowsky, and H. A. Atwater, “Three-dimensional nanoimprint lithography using two-photon lithography master samples,” pp. 1–4, 2017.

[2] D. Bodas and C. Khan-Malek, “Formation of more stable hydrophilic surfaces of PDMS by plasma and chemical treatments,” *Microelectron. Eng.*, vol. 83, no. 4-9 SPEC. ISS., pp. 1277–1279, 2006.

[3] S. Manzoor *et al.*, “Solar Energy Materials and Solar Cells Improved light management in planar silicon and perovskite solar cells using PDMS scattering layer,” *Sol. Energy Mater. Sol. Cells*, vol. 173, no. April, pp. 59–65, 2017.

[4] C. Lefky, A. Mamidanna, Y. Huang, and O. Hildreth, “Impact of solvent selection and temperature on porosity and resistance of printed self-reducing silver inks,” *Phys. Status Solidi Appl. Mater. Sci.*, vol. 213, no. 10, pp. 2751–2758, 2016.

[5] “No Title.” [Online]. Available: https://www.memsnet.org/about/processes/etch.html.

[6] A. P. Guide, “THE MICROSCOPE,” 1999.

[7] S. A. Technology, “Scanning Electron Microscope A To Z.”

[8] A. Force and M. Afm, “Basic Theory,” pp. 1–8.

[9] T. H. Effect, “2.7.5. The Hall Effect,” pp. 34–35.

[10] R. Green, “Hall Effect Measurements in Materials Characterization Who Needs to Measure Hall Effect ? Growing Interest in the Use of Hall Effect Measurements,” no. 440, pp. 1–12, 1879.

[11] A. Larsen and A. Larsen, “Forecasting mismatch losses : An empirical study investigating module level inverter- and string inverter systems,” pp. 1–34, 2014.

Chapter 4: Materials and Methodology

This study combines the microchannel approach with the use of a transparent flexible polymer i.e. Polydimethylsiloxane (PDMS) that is engraved with the contact grid design with a highly conductive, low temperature curing reactive silver ink (RSI) to form effective metal contacts with high transparency.

4.1 Synthesis of Reactive silver ink (RSI)

RSI was synthesized by adding 1g of silver acetate (Sigma Aldrich) into 2.5 mL of 32% aqueous ammonium hydroxide (Merck) which was vigorously mixed at room temperature, using a vortex mixer until the salt was dissolved. 0.2 mL of formic acid (Merck) was then added dropwise with constant vortex mixing after each drop. Change in color of the solution from light brown to greyish black indicates reduction of silver ions to large particles of silver. This solution was kept undisturbed for around 12 hours to allow the larger particles of Ag to settle out and then filtered using a 0.22 μm syringe filter, resulting in a clear ink solution containing 22wt% silver [1], [2].

4.2 Perovskite device fabrication

Perovskite solar cells were obtained from University of Stanford, USA and were fabricated as per the design for their champion tandem solar cells (Silicon/ Perovskite tandems) with a record efficiency of 23.6% [3]. Semitransparent single junction PVK cells were fabricated on ITO (170 nm) coated glass slides (0.7 mm) with a sheet resistivity of 10 Ω/□ glass from Xin Yan Technology. These slides were cleaned using sonication in Extran, isopropanol and acetone following a UV ozone treatment for 15 minutes. A 5 mg/mL solution of Poly[bis(4-phenyl) (2,4,6-trimethylphenyl)amine (PTAA) from Solaris, mixed in anhydrous chlorobenzene (Sigma-Aldrich) filtered through filtered using a 0.2 μm syringe filter was spin coated on to the ITO glass for 40 seconds at 4000 rpm, followed by annealing at 60°C to deposit a 15nm thick hole transport layer (HTL). The 500 nm thick layer of the perovskite $FA_{0.83}Cs_{0.17}$ $Pb(I_{0.17}$ $Br_{0.83})_3$ was deposited after cooling the PTAA to room temperature [4]. A stoichiometric solution containing formamidinium iodide (Dyesol), $PbBr_2$ (TCl) in a mixture of anhydrous *N*,*N*-dimethylformamide (DMF, Sigma-Aldrich) and dimethyl sulfoxide (DMSO, Sigma-Aldrich), PbI_2 (TCI), and CsI (Sigma-Aldrich, 99.99% trace metals) was dropped on top of the PTAA layer via a 0.2 μm PTFE filter for 10 seconds

at a spin rate of 1000 rpm (T_1, SPD_1), following rotation for 25 seconds at 6000 rpm (T_2,SPD_2) and finally for 5-7 seconds at 1000 rpm (T_3,SPD_3). The samples were treated with compressed dried air during the 3rd spin step, annealed at 60 °C on a hot plate for 5 seconds and then at 100°C for half an hour [5]. A 30 nm layer of C_{60} wes evaporated on top of the absorber, followed by 6 nm of SnO_2 which was deposited using pulsed-CVD at 100 °C and 2nm of zinc tin oxide (ZTO) at 100 °C was deposited for the semitransparent cells.

4.2.1 ITO deposition (ASU) DC magnetron sputtering

A 60nm thick layer of ITO was finally deposited via DC sputtering at Arizona State University, forming a topmost blue film. The ITO layer thickness was reduced to 60nm on purpose, to make it possible to quantify the effect of ETCs on the performance of perovskites. A commercially available Perkin-Elmer DC magnetron sputtering system (PE-4450) was used to deposit these ITO films. This system consists of a loading chamber and a process chamber, maintaining a constant base pressure of approximately 50 mTorr with the help of a mechanical pump (Edwards QDP 40) and a base pressure of <1 x 10-3 mTorr using a Cryo pump (CTI on board 8") for the respective chambers. The target was commercial grade, having purity >99.995 % and composition 90:10 (In_2O_3:SnO_2 wt.%). The sputtering gases used for the reactive sputtering of ITO were Argon and Oxygen, both of purity >99.995 % and the deposition rate was appx 12 nm/min. The process chamber was kept under vacuum of 2 mTorr and the Ar and O_2 flow rates were 4 sccm and 0.3 sccm respectively. The target surface was preconditioned for 30 minutes [3].

4.3 Polydimethylsiloxane (PDMS) stamp

A polydimethylsiloxane stamp, engraved with the triangular microchannel grooves was received on request from California Institute of Technology, USA. This stamp was made using a master mold made of a silicon wafer using two photon lithography [6]. Sylgard 184 silicone elastomer was used to make the PDMS solution with a 10:1 polymer base to curing agent ratio. A vacuum desiccator was used to ensure no bubbles were trapped in the mixture, which was then poured on top of the master mold placed in a petri dish and cured at 100°C for 1 hour. This 4-inch diameter stamp was allowed to cool and the pulled off the master mold. Pitch of the fingers i.e. the distance between each individual grid finger was 75 um and the dimensions are shown in the SEM images below.

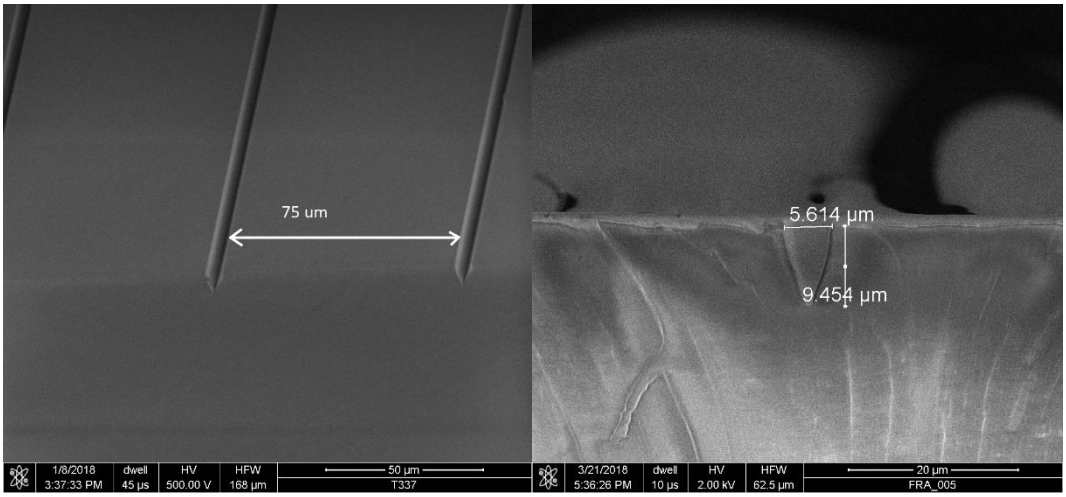

Figure 11 a) SEM image of ETC engraved PDMS stamp showing pitch of contact grid b) cross-sectional SEM of the triangular grid finger

4.3.1 Pretreatment of substrate and stamp

1 x 1 cm^2 pieces of the PDMS stamp were cut using a clean, sharp blade and dipped in isopropanol for 4-6 hours. This pretreatment is necessary to remove any grease, moisture or debris on the polymer that may impede effective adhesion of the stamp with the substrate. In case of bare and FTO coated glass slides, acetone rinsing was followed by dipping the glass slides in IPA for 30 minutes to ensure a clean surface.

4.3.2 Plasma treatment of substrate and stamp

The plasma treatment was conducted in a reactive ion etching (RIE) system that uses an RF power supply for generating plasma. For oxygen plasma modification, flow rate of oxygen and pressure of the system was kept constant. A mixture of Argon and Air in the ratio 1:2 was used for this purpose and the plasma was generated at medium power once the vacuum reaches the mTorr regime. PDMS and glass substrates were placed inside the plasma chamber and treated at medium power for 5-10 minutes. The plasma reacts with the glass and the polymer to create silicon atoms that have one missing electron on their exposed surface. Once the substrate and stamp undergo plasma treatment, these silicon dangling bonds combine with a hydrogen and create Si-OH bonds on the surface of both components. As the polydimethylsiloxane block is adhered to the glass slide, a covalent bond is formed between the two i.e. Si-O-Si. This step ensures a tight seal between the PDMS stamp and substrate with strength of the surface bonding between the glass and the PDMS reaching 75psi [7]. Another important function of the plasma treatment is to induce hydrophilicity and increase the affinity of both substrates to allow the ink to pass over them.

4.4 Dilution of Reactive Silver Ink

The reactive silver ink on its own has very low viscosity and low wettability. Both the polymer stamp (PDMS) and glass substrate are hydrophobic and even though plasma treatment renders them somewhat hydrophilic, the low viscosity of RSI impedes effective flow of the conductive liquid into the microchannel grid. Lefky, et al. studied the effect of adding solvents in different ratios with the RSI [8]. Ethanol was added in ratios 1:5 and 1:10 (RSI:Ethanol) to study the effect on chemical sintering and porosity of the silver upon reduction and annealing.

4.4.1 Deposition of conductive films for resistivity measurements

Bare glass slides (9mm x 9mm) were, rinsed with acetone and dipped in IPA for 3-4 hours. They were subjected to plasma treatment afterwards for improving adhesion. A commercial silver conductive paste (Sigma Aldrich – 735825) was deposited on one of the bare glass slides with a metal spatula and annealed at 150°C for 1 hour. The composite mixture of the diluted reactive silver ink and commercial paste (5:1) was deposited on another glass slide via spin coating, 100 ul of the solution was dropped and spun at 1000 rpm for 12 sec (T1, SPD1) and then at 18000 rpm for 30 sec (T2, SPD2). The composite was annealed at 100°C for one hour in a vacuum oven. 150 ul of the RSI was spin coated on a bare glass slide at the same spin coating conditions and heated in the drying oven at 100°C for 30 minutes. A textured silicon wafer with a DC-sputtered ITO layer was also used as reference.

4.5 Injection of RSI via capillary action

Once the plasma treatment of the PDMS and glass substrates was complete, the polymer was inverted immediately on top of the respective substrates; 1) bare glass slide 2) FTO coated glass slide and 3) perovskite solar cell. This step should be carried out immediately because the surfaces lose their reactivity as the effect of plasma treatment wears off, diminishing the adhesive effect within 5-10 minutes of exposure to the external environment. Once a tight seal was ensured between the stamp and substrate, the conductive mixture (both dilute RSI and Ag paste + RSI composite) was injected using a micropipette (2-20 ul) and almost 3 ul of ink was injected into each stamp. Both conductive mixtures travelled through the ETCs' microchannels via capillary action, which is effective only up to a distance of a few millimeters [9].

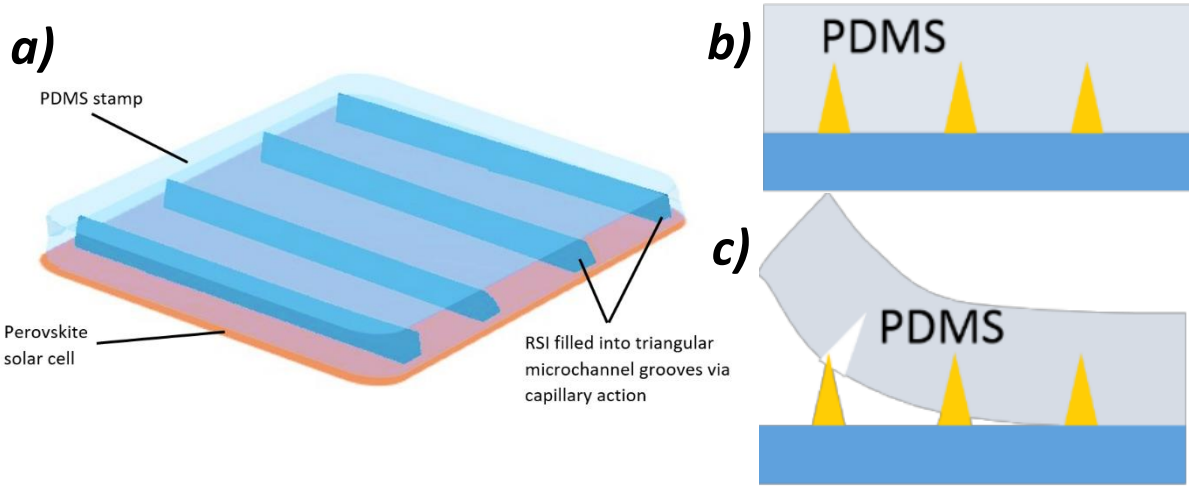

Figure 12 Schematic diagram of methodology a) PDMS placed on top of substrate is filled RSI through the open ends of the microchannel grooves b) The ink is allowed to cure c) The stamp is peeled to reveal the effectively transparent contacts.

4.5.1 Curing and annealing of the ETCs

The stamp was left on the substrate for over 24 hours to let the conductive mixture cure at room temperature [10], after which it was removed and the ETCs were annealed at around 100ºC for the bare glass slide and FTO coated glass slide, and 60ºC for the perovskite solar cell substrate (since PVKs are highly sensitive to temperature). Fig 13. shows SEM images of the ETCs. The images clearly show that the undiluted reactive silver ink a) and b) results in highly porous, discontinuous and poorly connected structures, whereas a visible improvement is seen in the case of the diluted (five parts and ten parts ethanol) reactive silver ink structures, which show significantly larger cluster size, higher continuity and far improved chemical sintering. This improvement can be attributed to the fact the addition of ethanol increases the curing time of the ink, allowing ample time for nuclie formation.

4.6 Formation of Reactive Silver Ink and Silver paste composite

The reactive silver ink on its own, has very little silver content, not enough to fill the microchannel grooves completely and retain the shape of the mould, hence a commercial silver paste of moderate curing temperature was added to form a composite that would have high conductivity and cure at relatively lower temperature (~120-150ºC). The Ag paste used was added 1 part to 5 parts of the already diluted reactive silver ink (1:10 RSI:EtOH). Fig 15 shows optical images of ETCs formed using the diluted reactive silver ink (1:10 RSI:EtOH) and those formed with the RSI-Ag paste composite (5:1 RSI:Ag paste).

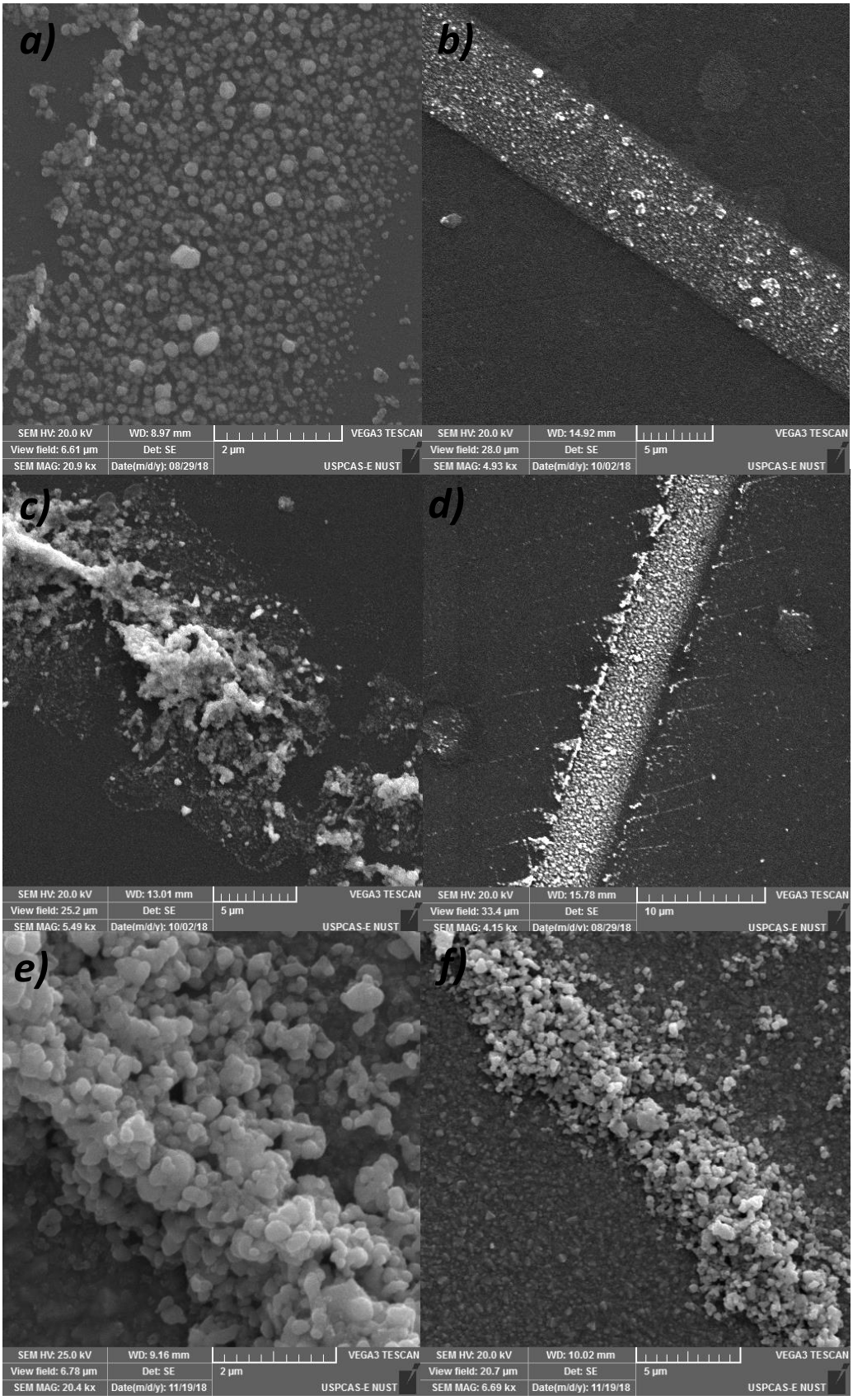

Figure 13 SEM images of ETC deposited using RSI having 2 parts ethanol a) and b) 5 parts ethano) c) and d) and 10 parts ethanol e) and f).

Optical images of the ETCs deposited using the diluted ink (1:10 RSI:EtOH) and the Ag-paste composite are shown below for comparison (Fig 14). Despite showing much better performance in terms of compatibility with this technique, the 1:10 RSI:EtOH ink shows poor connectivity and is not all of the fingers in the grid are deposited all the way through.

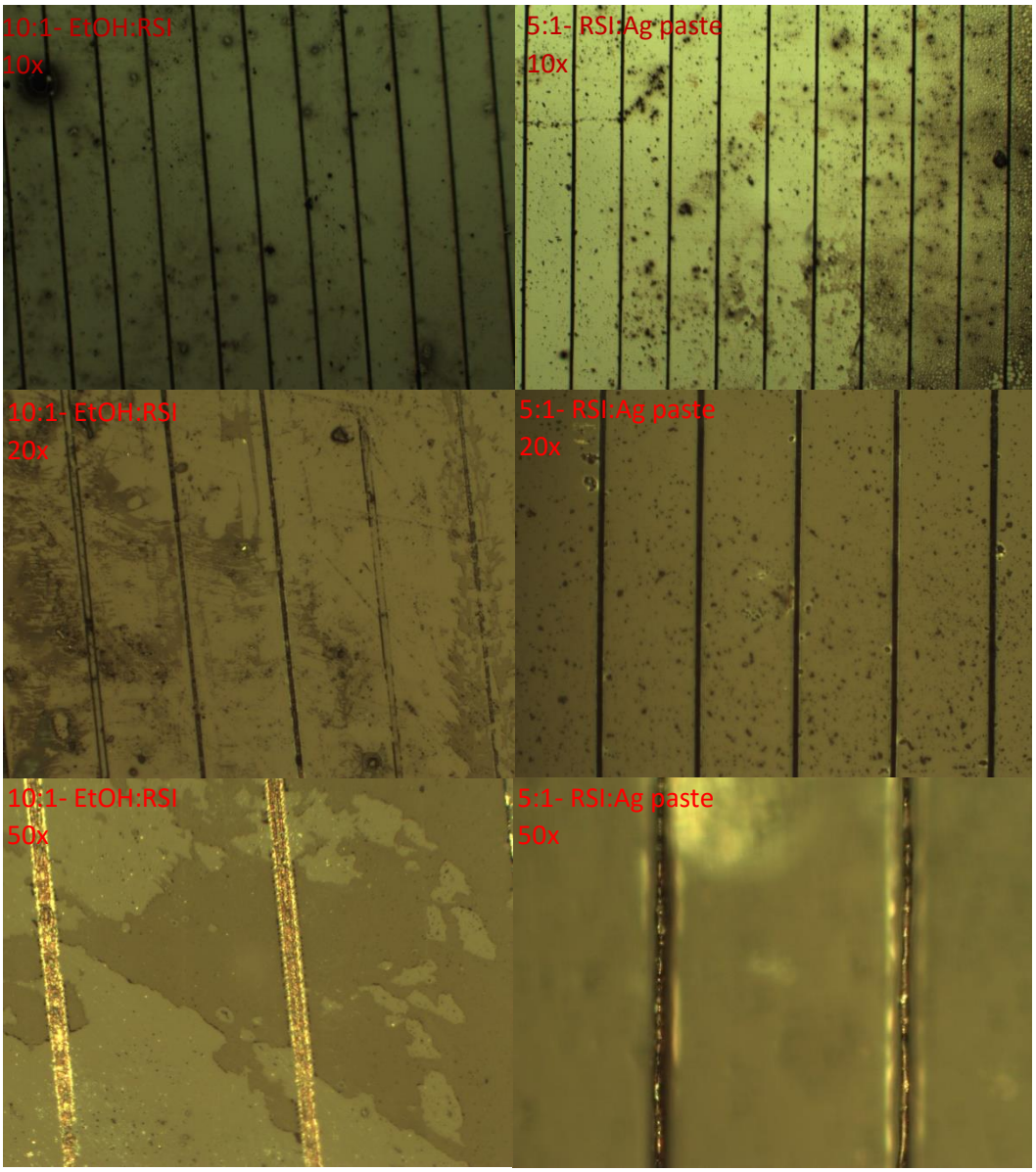

Figure 14 Optical images of RSI (10 parts ethanol) deposited ETC

However, the RSI-Ag (5:1) composite shows much better features that hold a rigid three-dimensional structure throughout the grid. Fig 15 shows SEM images of ETCs deposited using the RSI-Ag composite. The two fingers are a part of two separate grids, for one a) the PDMS stamp was pulled away after curing and the other b) was cured after the stamp was peeled off.

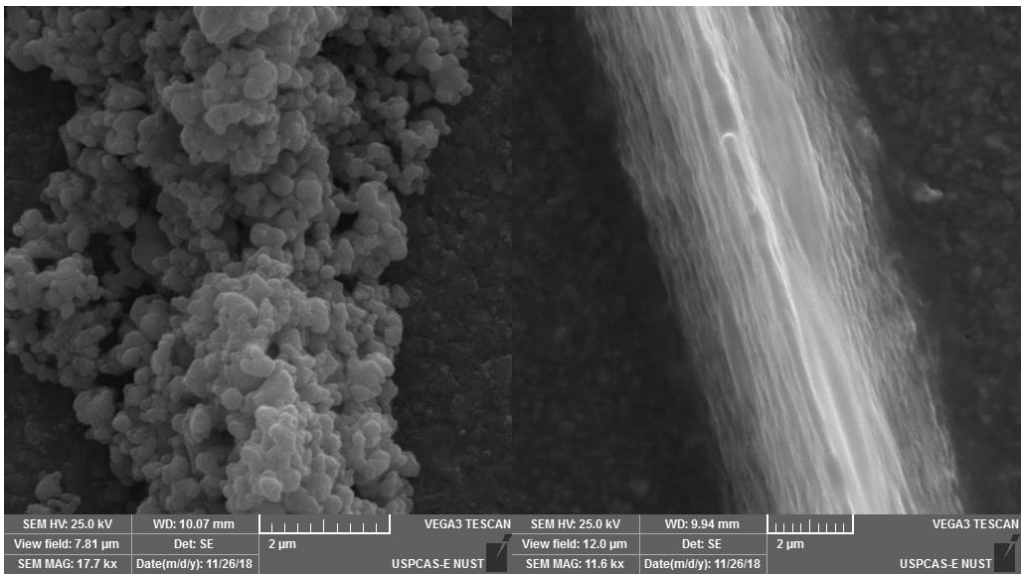

Figure 15 SEM images of a) poorly deposited ETC b) highly chemically sintered ETC.

4.7 Atomic Force Microscopy images of the ETCs

Four samples of effectively transparent contacts deposited using four different ink compositions were subjected to atomic force microscopy and the resulting images are shown in Fig 16. The images clearly depict expected results in which the ETC grid formed using undiluted reactive silver ink Fig 16 a) show a very shallow and hollow structure, the maximum height for this was found to be 532nm as opposed to the expected 9.454um height of the triangular cross-section grooves. For the five-parts ethanol sample b) some improvement is seen in that more Ag is evidently deposited, however, even this structure was hollow to quite some extent and the maximum height was measured as 1.09um. Further improvement is seen for the ten-parts ethanol diluted reactive silver ink c) in which there is a visible three-dimensional structure and the height is measured as 2.05um. However, the best results are seen for the composite (RSI-Ag paste) deposited ETCs, for which we can see a definite rigid structure that conforms to the triangular cross-section mold used for its fabrication. The maximum height for this structure was determined to be ~4um.

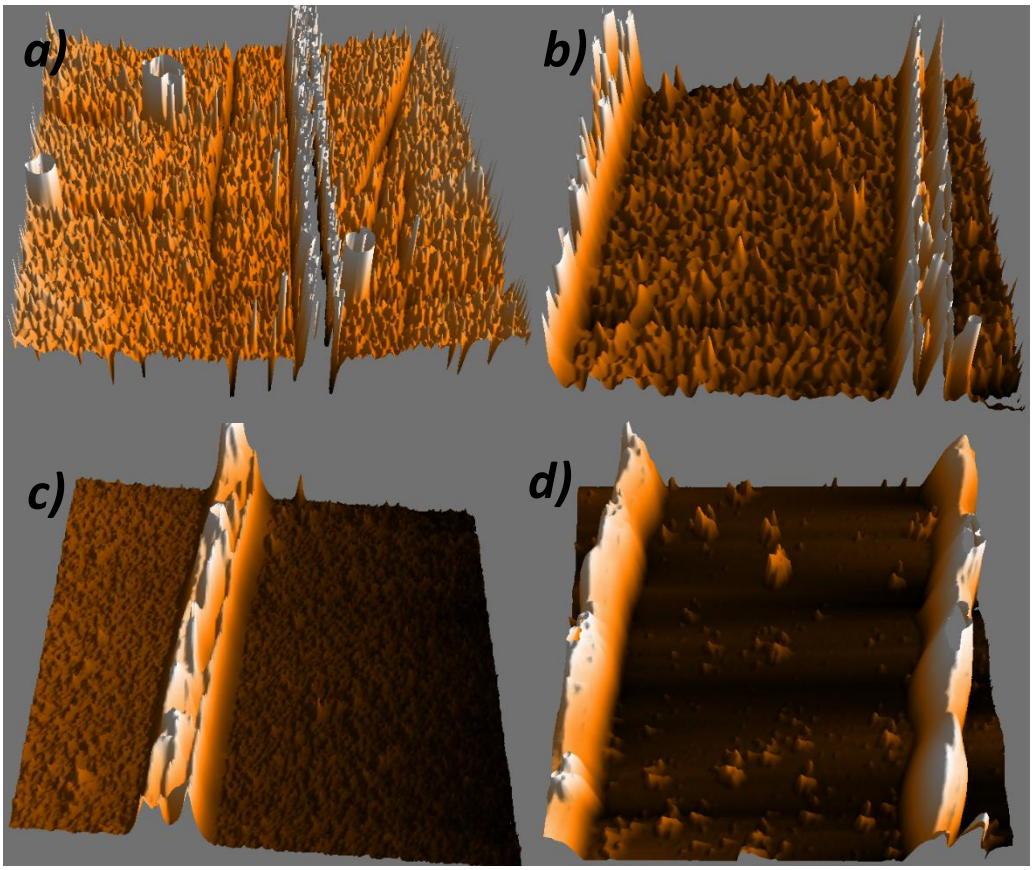

Figure 16 AFM images of ETC deposited using a) Undiluted RSI b) 1:5 RSI:EtOH c) 1:10 RSI:EtOH and d) 5:1 RSI:Ag-paste

4.8 Deposition of conductive films for resistivity measurements

Bare glass slides (9mm x 9mm) were, rinsed with acetone and dipped in IPA for 3-4 hours. They were subjected to plasma treatment afterwards for improving adhesion. A commercial silver conductive paste (Sigma Aldrich – 735825) was deposited on one of the bare glass slides with a metal spatula and annealed at 150°C for 1 hour. The composite mixture of the diluted reactive silver ink and commercial paste (5:1) was deposited on another glass slide via spin coating, 100 ul of the solution was dropped and spun at 1000 rpm for 12 sec (T1, SPD1) and then at 18000 rpm for 30 sec (T2, SPD2). The composite was annealed at 100°C for one hour in a vacuum oven. 150 ul of the RSI was spin coated on a bare glass slide at the same spin coating conditions and heated in the drying oven at 100°C for 30 minutes. A textured silicon wafer with a DC-sputtered ITO layer was also used as reference.

4.9 Summary

In this chapter we discuss the detailed methodology and approach along with the materials and methods used in this study, the various changes and adaptations that were made during the course of this research for achieving the desired results. The microchannel approach was basically designed for developing contacts for thin film solar cells. Various compositional changes were made to the low temperature reactive silver ink t compensate for the loss in conductivity due to poor connectivity exhibited by the structures. The results showed that the RSI showed improvement in connectivity and cluster formation upon dilution with polar protic solvent, Ethanol. However, the composite formed by mixing the RSI with a commercial Ag paste showed the best performance in terms of conforming to the desired structures and exhibited far better chemical sintering.

References

[1] S. B. Walker and J. A. Lewis, “Reactive Silver Inks for Patterning High-Conductivity Features at Mild Temperatures,” no. I, pp. 2011–2013, 2012.

[2] S. B. Walker and J. A. Lewis, “Reactive silver inks for patterning high-conductivity features at mild temperatures,” *J. Am. Chem. Soc.*, vol. 134, no. 3, pp. 1419–1421, 2012.

[3] K. A. Bush *et al.*, “23.6%-Efficient Monolithic Perovskite/Silicon Tandem Solar Cells With Improved Stability,” *Nat. Energy*, vol. 2, no. 4, pp. 1–7, 2017.

[4] K. A. Bush *et al.*, “Compositional Engineering for Efficient Wide Band Gap Perovskites with Improved Stability to Photoinduced Phase Segregation,” *ACS Energy Lett.*, vol. 3, no. 2, pp. 428–435, 2018.

[5] G. E. Eperon *et al.*, “Perovskite-perovskite tandem photovoltaics with optimized band gaps,” *Science (80-.).*, vol. 354, no. 6314, pp. 861–865, 2016.

[6] R. Saive, C. R. Bukowsky, and H. A. Atwater, “Three-dimensional nanoimprint lithography using two-photon lithography master samples,” pp. 1–4, 2017.

[7] A. Note, “Plasma Treated PDMS for improved bonding performance of microfluidic devices Plasma Treated PDMS for improved bonding performance of microfluidic devices,” vol. 44, no. 0, pp. 0–5, 1925.

[8] C. Lefky, A. Mamidanna, Y. Huang, and O. Hildreth, “Impact of solvent selection and temperature on porosity and resistance of printed self-reducing silver inks,” *Phys. Status Solidi Appl. Mater. Sci.*, vol. 213, no. 10, pp. 2751–2758, 2016.

[9] R. Saive *et al.*, “Sustainable Energy & Fuels Silicon heterojunction solar cells with e ff ectively transparent front contacts,” *Sustain. Energy Fuels*, vol. 00, pp. 1–6, 2017.

[10] A. M. Jeffries, A. Mamidanna, L. Ding, O. J. Hildreth, and M. I. Bertoni, “Low-Temperature Drop-on-Demand Reactive Silver Inks for Solar Cell Front-Grid Metallization,” vol. 7, no. 1, pp. 37–43, 2017.

Chapter 5: Conclusions and Recommendations

5.1 Thermogravimetric analysis of the Reactive Silver Ink (RSI)

Thermogravimetric analysis of the ink was carried out at 90ºC (curing temperature) for 30 minutes at a ramp rate of 10ºC/ min and the ink showed stable behavior with only a 0.85% loss in weight. It is stable at room temperature and can be stored at lower temperatures for many weeks. When heated up to 500 ºC at a ramp rate of 10ºC/min, the ink showed highly stable behavior up to around 160ºC after which there is a rapid increase in mass percentage loss, reaching a maximum of 9.74% at 500 ºC.

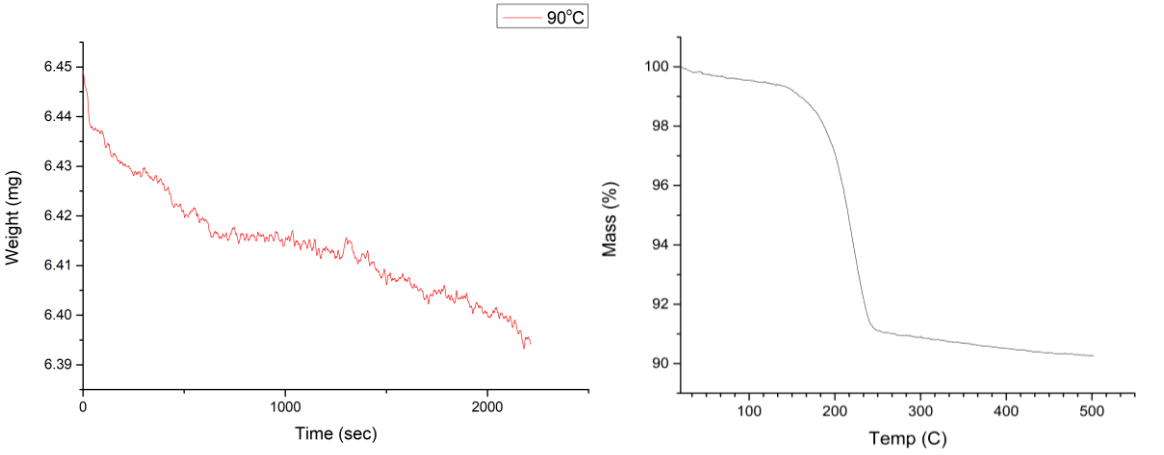

Figure 17 Thermogravimetric analysis of reactive silver ink a) at 90ºC b) at 500 ºC with a ramp rate of 10 ºC/min

5.2 UV-Visible Spectroscopy of Reactive Silver Ink (RSI)

Absorption spectrum of the RSI shows an absence of absorption in the 400-425 range, which is typically attributes to the presence of silver particles, hence proving that the ink is in fact particle free. Tollen's reagent shows the characteristic peak around this region, however no such peak can be observed for the modified Tollen's reagent (reactive silver ink) synthesized in this study.

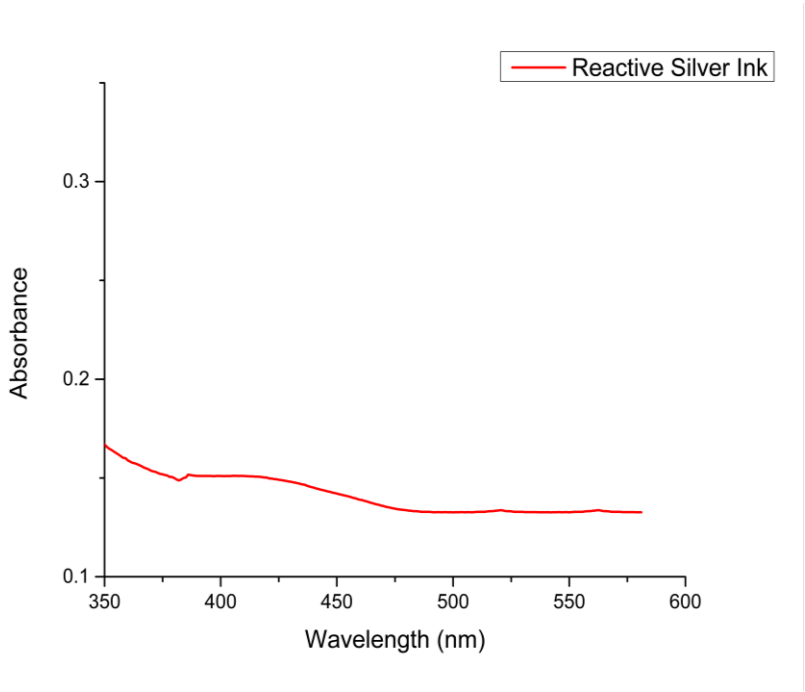

Figure 18 Absorbance spectrum of Reactive Silver Ink using UV-VIS spectroscopy

5.3 Hall effect measurements of conductive films

Hall effect measurements of the above samples were carried out for the films prepared as described in section 4.7 and the resultant sheet resistivity, resistivity and conductivity are presented in Table 4.1.

Table 1 Hall effect measurements of conductive materials used

Sr. no	Conductive material	Current (I)	Sheet resistivity ($\Omega/\square$)	Resistivity (Ω .cm)	Conductivity ($1/\ \Omega.cm$)
1.	**Ag paste**	1mA	$1.105x10^{-2}$	$5.526x10^{-4}$	$1.774x10^{3}$
2.	**RSI (undiluted)**	1mA	$1.42x10^{2}$	$4.25x10^{-1}$	$2.36x10^{0}$
3.	**Dilute RSI (10:5)**	1mA	$4.569x10^{0}$	$4.569x10^{-3}$	$2.189x10^{2}$
4.	**Dilute RSI (10:1)**	1mA	$4.992x10^{0}$	$1.248x10^{-4}$	$8.01x10^{2}$
5.	**Ag paste + RSI (1:5)**	1mA	$7.798x10^{-2}$	$3.899x10^{-4}$	$2.565x10^{3}$
6.	**ITO on wafer**	1mA	$7.217x10^{-1}$	$7.217x10^{-4}$	$1.386x1^{3}$

From the table it can be deduced that the improved chemical sintering and continuity of the ETCs with the increase in dilution contributes to the improvement in electrical properties. A comparison of the R_s, ρ and σ values of the respective films shows that the conductive performance of the RSI and Ag paste composite (1:5) is comparable to

that of the pure Ag paste. Which means that the composite will show comparable performance when used to fabricate the grid. The pure conductive paste cannot be used as such for this process because of its high viscosity which hinders the capillary action, moreover, dilution reduces the cost of the conductive solution being used. The value of resistivity reported for the commercial paste used is 1-3 x 10^{-5} Ω-cm and that for the RSI in literature is 10^{-4} Ω-cm [1]. The reduction in performance can be attributed to improper storage conditions of the paste, which requires refrigeration at 2 - 8°C. Reactive silver ink alone does not show good conduction, this is mostly due to the highly porous nature of the ink which shows poor chemical sintering upon drying. The high solvent content (ammonium hydroxide and ethanol) means that the ink requires slow and gradual heating to avoid rapid evaporation, leading to highly porous structures that exhibit low connectivity. This porosity contributes to poor conduction, since for a structure to be highly conductive it must have high connectivity and chemical sintering.

5.3.1 Effect of varying composition of RSI on film quality

When the reactive silver ink was used in its original composition, the deposited features showed high porosity and very poor chemical sintering, so it was mixed with various ratios of ethanol to determine the best possible composition for obtaining highly uniform and non-porous ETCs. The addition of ethanol also increased the viscosity of the ink, which helped improve the capillary effect, required for dissemination of the conductive liquid through the PDMS stamp. RSI with 10 parts ethanol showed the best chemical sintering and lowest porosity as can be seen in Fig 13. However, the porosity of the RSI would still be a problem because of the miniscule dimensions of the grid fingers. Mixing the diluted RSI with a conductive silver paste increases the viscosity of the liquid and improves the flow via capillary action along with dramatically enhancing the chemical sintering and compactness of the individual fingers. Various ratios of the ink and paste mixture were tested for performance and compatibility with this technique, mostly to increase the silver content in the mixture, as the RSI alone would form highly porous structure with very little silver content once the solvent evaporates. RSI in ethanol in a 10:1 ratio which showed the best chemical sintering without compromising the capillary motion was mixed with the commercial Ag conductive paste (Sigma Aldrich) in a 1:5 ratio (Ag paste: RSI).

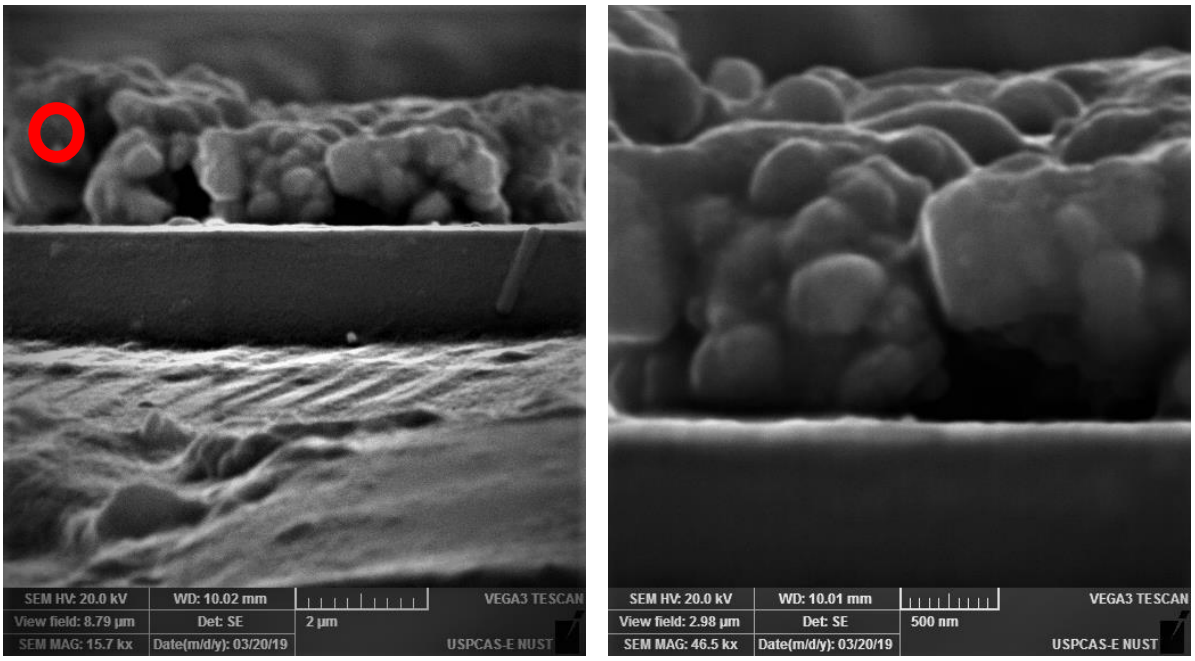

Figure 19 SEM images of the film deposited using RSI:Ag paste composite

5.4 Transmittance of the ETC grids

UV-Vis spectroscopy was used to measure the transmittance of the ETC grid deposited on a glass slide. For a metal contact to be effective, it must have high transmittance. ITO usually exhibits excellent transmittance of more than 90% in the visible region. For the ETCs to be comparable to ITO in optical properties, they must exhibit low parasitic absorption and high transmittance. The transmitance spectrum of the ETC deposited using RSI on bare glass slides is given below followed by a transmittance spectrum comparison for bare ITO with ETC deposited ITO .

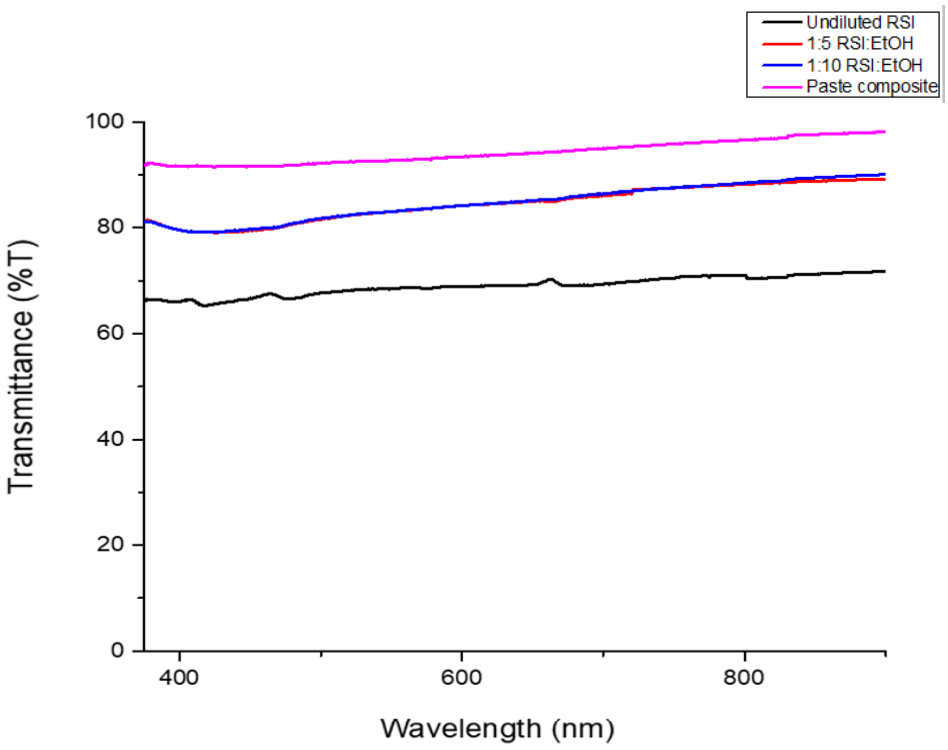

Figure 20 Transmittance spectra of effectively transparent contacts deposited using various compositions of reactive silver ink

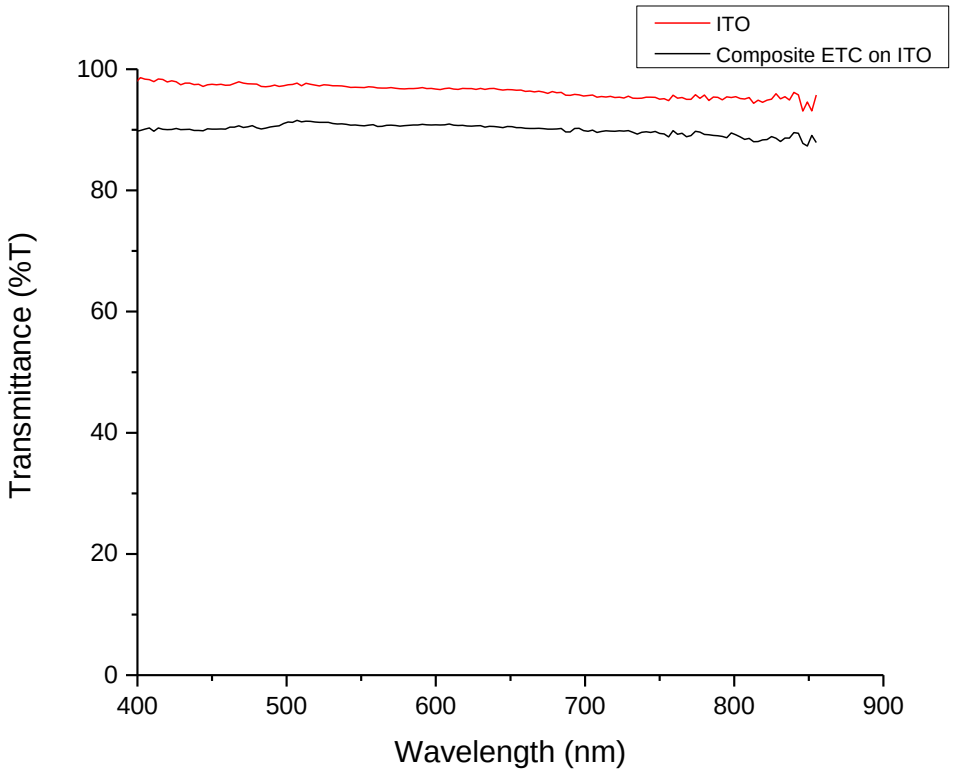

Figure 21 Comparison of transmittance of ITO coated glass and ETC (RSI:Ag composite) deposited on ITO coated glass

5.5 Effectively transparent contacts for perovskite solar cells

Perovskite solar cells were requested and obtained from Stanford University. IV-measurements for these cells were carried out and are given in table. The unusual shape of the IV curve for the perovskite solar cells can be attributed to series resistance. Degradation of the perovskite solar cells as a result of interaction of the polar protic solvent (in the RSI) lead to an evident decrease in the V_{oc}, which can be attributed to higher values of series resistance, resulting from damage in the absorber and ITO layers. Current density calculations show an improvement in some of the cells, this can be explained based on the fact that charge collection is improved upon deposition of the ETC in addition to the thin ITO layer (60nm). This ITO layer was basically deposited to assist charge collection by the ETC. As mentioned earlier, if the fingers are placed closely they can remove the need for ITO as an assistive layer.

Table 2 IV measurements for perovskites before and after deposition of ETCs

	Without ETC			With ETC		
Cell ID	V_{OC} (V)	J_{SC} (mA)	FF (%)	V_{OC} (V)	J_{SC} (mA)	FF (%)
DC-1	1.069	11.9	29.5	1.013	17.896	35.1
DC-8	0.626`	6.54	26.2	0.404	12.3582	25.7
DC-15	0.869	7.3	26.9	0.761	19	25.5
DC-11	0.525	7.38	26	0.523	5.2	26.8
DC-12	0.07	3.53	25	0.039	5.17	25

5.5.1 Degradation of perovskite solar cells with RSI:Ag paste composite

When ETCs were deposited on the perovskite solar cells, they resulted in degradation of the ITO and absorber layer. This damage is attributed to the interaction of organic cations in the absorber layer (i.e. methyl ammonium, formamidinium) with the polar protic solvent (ethanol) in the ink composite. The hydrogen bonds in the protic solvent reacts with these cations and dissolve easily, leaving behind a yellow layer of the degraded absorber. IV-measurements for these cells were carried out and the active area was calculated using MATLAB for more precise calculations of the device performance parameters, particularly the current density (J_{sc}). The results depicted do not show any improvement in performance because of the severe device degradation.

5.5.2 Causes for abnormal behavior of PVK

From the results, it is clear that there is a significant decrease in the V_{oc} of the cells after deposition of ETC, whereas the J_{sc} is seen to increase the cells. Deviation of the IV-curve from normal behavior such that the V_{oc} and FF of the cell are affected, can

be caused by a number of factors, most likely an increase in the series resistance (R_{series}), and decrease in the shunt resistance (R_{sh}). R_{sh} depicts any parallel path of high conductivity (shunt) at any of the interfaces between the different layers or on the edges of the perovskite solar cell and can have a major effect on the performance of the cell. Perovskite films often consist of many pinholes due to which the contact between electron and hole transporting layers provides low resistance paths, leading to decrease in the fill factor and open-circuit voltage. The shunt paths direct the current away from the intended path and cause a detrimental effect to the solar cell performance. The normal values for R_{sh} lie between 2000-4000 ohm, however, those measured for the perovskite solar cells using the one sun solar simulator were as low as ~100 ohms. Reduction in the shunt resistance can result in power loss of as much as 63% [2]. Series resistance for PVK solar cells should be low, of the order of 1-5 ohm, however, when measured for these cells, it was observed to be in the range 50-200 ohm. This can be attributed to the resistance between the charge transport layers and the metal-semiconductor contact. Both of these factors reduce the fill factor, and open circuit voltage.

5.6 Ink usage

Measurement of surface area coverage by the microscale ETC grid showed that 0.06961cm^2 out of the total 1cm^2 (area of the stamp) was covered with ink using this particular grid design, which is a mere 6.961% of the total stamp area. The size of the cells used (area covered by ITO) was 1.3cm^2. Considering the whole ITO covered area as the active cell. There are approximately 124 fingers per 1 cm^2 of stamp, the total volume of these grid fingers is appx 2.653×10^{-7} cm^3 of ink per groove, meaning almost 3.289×10^{-5} cm^3 of ink is required per 1cm^2 stamp (0.003289720 ul). This is much less than the conductive ink/paste requirements by a conventional screen-printing method.

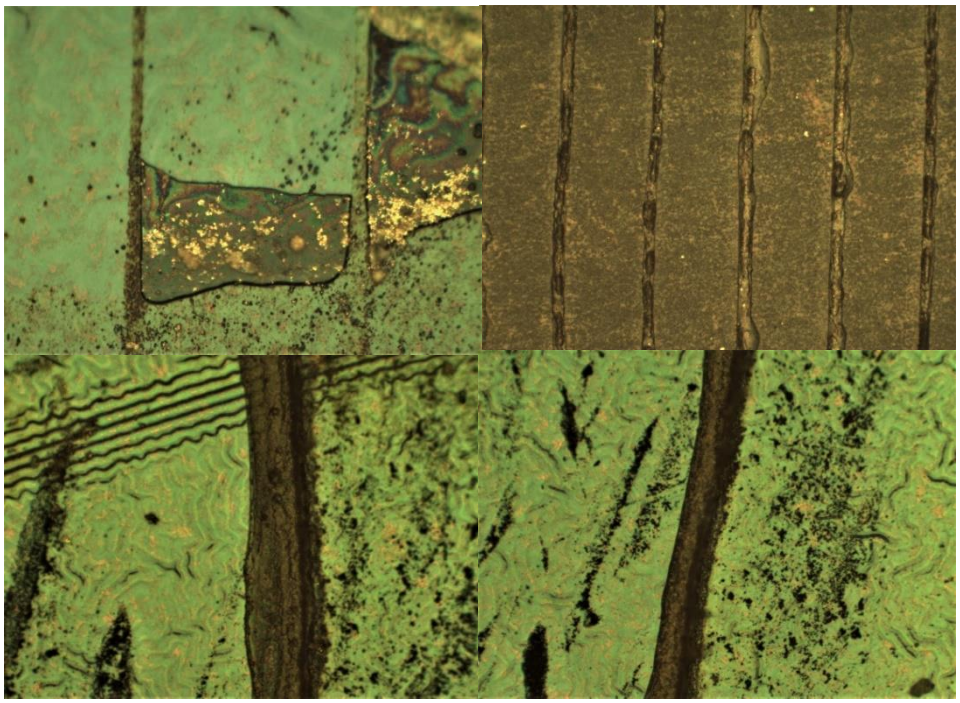

Figure 22 Optical microscope images of PVK solar cells after deposition of ETC a) damaged ITO after dissolving in protic solvent (RSI) b) poorly deposited ETC c) and d) individual grid finger

5.7 Light trapping and reflection by ETC

Examining a cross-section of the grid fingers shows us that the triangular grooves are inclined at an angle of approximately 73.5º. Rebecca *et al*. carried out simulations for various angles of incidence and percentage of surface area coverage by ETC [3]. At 0º, the results show that ETCs performs optically the same way as for cells without a contact grid, for incident angles parallel to the grid fingers there were still no significant losses exhibited. However, for angles perpendicular to the grid fingers (along the y-axis) there is a visible decrease in J_{sc} at particular angles as the coverage increases. For high surface area coverage and greater angle of incidence, incident light is likely to be reflected away from the active cell area towards other gird finger lines.

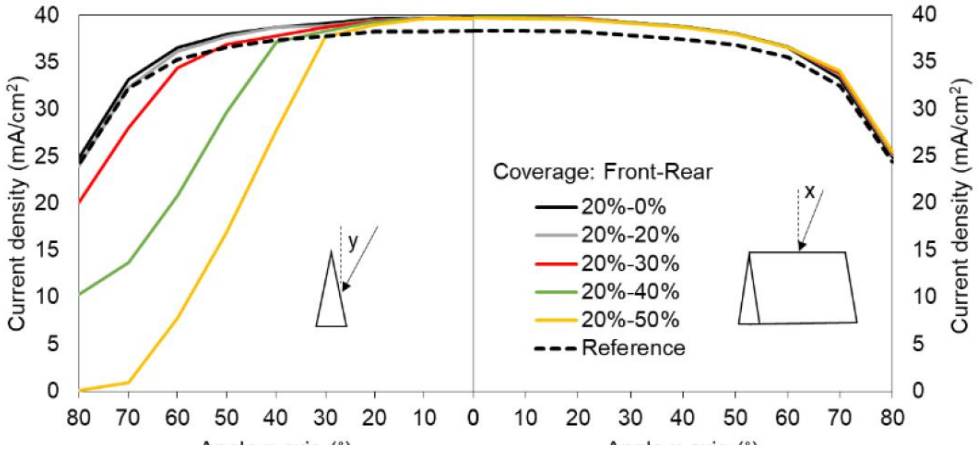

Figure 23 Generated current density for rear side illumination without cosine factor depending on the ETC rear coverage and on the angle of incidence for an ETC front coverage of 20% [50].

5.8 Recovery of ITO

As evident by the effect of ethanol containing RSI (10:1), polar protic solvents can dissolve the organic cation containing perovskite absorber layer. Using nitric acid, it was possible to remove all the layers. Previously, recycling of ITO had been studied with various non-polar (Diethyl ether, Chlorobenzene ,Toluene), polar protic (IPA, Methanol, Water) and polar aprotic solvents (DMF, GBL and Acetone) on a perovskite solar cell (SpiroMeOTAD/MALI/mp-TiO2/TCG). The non-polar solvents were only able to dissolve the SpiroMeOTAD hole transport layer, exposing the absorber layer. The polar protic solvents were able to partially dissolve the MALI absorber layer without removing the hole transport layer, whereas the ITO was successfully recovered using polar aprotic solvents. Nitric acid (68%) is a polar protic solvent which was used dissolve the different layers of the perovskite solar cell (ITO/PTAA/ $FA_{0.83}Cs_{0.17}$ $Pb(I_{0.17}$ $Br_{0.83})_3/C_{60}/SnO_2$/ZTO/ITO/ETC). It was able to remove all the successive layers down to the hole transport layer (PTAA), leaving behind the glass slide coated with ITO (170nm). 4-probe conductivity measurements showed that the ITO layer still had a sheet resistivity, Rs of 10 Ω/□. Nitric acid works just as well for the removal of successive layers of the pvk solar cell, as does DMF. However, the cost comparison shows that Nitric acid ($462/ton) costs much less as compare to DMF (appx $700-800/ton).

5.9 Summary

We have demonstrated effectively transparent contacts on a number of substrates and finally deposited them on perovskites. These microscale triangular prism shaped fingers have high transparency, comparable to ITO and can effectively conduct the charge carriers, enhancing the charge collection efficiency of the device. However, it was noticed that the conductive inks (RSI and Ag+RSI composite) used to deposit the ETCs caused a degradation of the subsequent layers of the PVK solar cell. This is due to interaction of the polar protic solvent with the organic cations (formamidinium) in the absorber layer [$FA_{0.83}Cs_{0.17}$ $Pb(I_{0.17}$ $Br_{0.83})_3$]. This metal grid design ensures low resistance, decreased shading and improved Ag usage.

References

[1] S. B. Walker and J. A. Lewis, “Reactive silver inks for patterning high-conductivity features at mild temperatures,” *J. Am. Chem. Soc.*, vol. 134, no. 3, pp. 1419–1421, 2012.

[2] E. L. Meyer and E. E. Van Dyk, “THE EFFECT OF REDUCED SHUNT RESISTANCE AND SHADING ON PHOTOVOLTAIC,” pp. 1331–1334, 2005.

[3] R. Saive, T. C. R. Russell, and H. A. Atwater, “Light Trapping in Bifacial Solar Modules Using Effectively Transparent Contacts (ETCs),” pp. 2–5.

Chapter 6: Conclusions and Recommendations

6.1 Conclusions

For thin film solar cells, the trade-off between the optical and resistive losses of the metal contact is perhaps the most crucial aspect that needs to be considered while trying to achieve an effective grid design. We have demonstrated the potential of effectively transparent contacts (ETCs) developed using low temperature reactive silver ink (RSI) along with a commercial Ag ink composite, to reduce losses incurred by the front grid metallization in solar cells. The ETCs achieve this by minimizing shadowing losses; owing to their high aspect ratio, reflective losses; because of the triangular cross-section of the fingers that helps redirect the incident light on to the absorber layer and resistive losses; which are overcome by using a highly conductive composite. They can effectively reduce the grid resistance, improve charge collection and Ag usage. These high aspect ratio Ag fingers, if placed close enough, can remove the need for TCOs completely. However, ITO if removed completely may induce instability to the PSC because it's presence acts as a barrier to the external environment and improves stability.

High aspect ratio of the fingers minimizes the shading losses. Moreover, the triangular prism shaped metal contact fingers along with the angle of incidence of incoming light can maximize light harvesting. The ETCs work to redirect incoming light on to the active cell surface. Even though their use is not limited to any photovoltaic or optoelectronic device, the compatibility of this technique with a low temperature curing ink makes them the ideal candidates for use in thermally sensitive solar cells like perovskites and Si heterojunction cells. One of the major challenges to this technique is the formation of large pores during rapid evaporation of solvent upon curing in case of the reactive silver ink. This is because of the high solvent content in the ink, which upon evaporation, leaves behind a highly porous, discontinuous structure, that poorly conducts electric current. Mixing the RSI with a commercial silver paste resulted in an increase in the silver content and higher viscosity, aiding the capillary action which this technique relies on for dissemination of the conductive fluid. These low-temperature curing ETCs formed using the reactive silver ink have

great potential for replacing the conventional screen-printed silver grid fingers in many PV applications.

6.2 Recommendations

The novel effectively transparent contacts intended for use with a low temperature curing conductive ink can successfully reduce the optical, reflective and resistive losses that are faced by the conventional metal contacts. They have previously been demonstrated for use with regular and bifacial silicon heterojunction solar cells. In this work, we have demonstrated their us on perovskite solar cells. However, due to the polar protic nature of the solvent present in the high conductivity composite used to deposit the ETCs, ITO and absorber layer of the PVK undergoes degradation wherever the solvent comes into contact with these surfaces, reducing overall performance of the cell. Electrochemical Impedance spectroscopy can be carried out to analyze the internal electrical processes that take place in the PVK solar cell and investigate the associated parameters quantitative and qualitatively. This technique should be used to analyze the degradation effects of the Ag ink composite on the different layers in the cell to give us a better understanding of parameters like recombination resistance, transport resistance, capacitive behavior and charge transport kinetics.

Moreover, effect of variation in the grid dimensions to develop the best design for any solar cell can lead to improved performance. These contacts are suitable for use with silicon heterojunction, bifacial silicon heterojunction, perovskite and Si/PVK tandem solar cells.

ICRANET2018-180146

Effectively Transparent Contacts With Low Temperature Reactive Silver Ink

Maria Kanwal
US Pakistan Center for Advanced Studies in Energy
National University of Science and Technology
H-12, Islamabad
Kanwal896@gmail.com

Nadia Shahzad
US Pakistan Center for Advanced Studies in Energy
National University of Science and Technology
H-12, Islamabad
nadia@uspcase.nust.edu.pk

Salman Mansoor
School of Electrical, Computer, and Energy Engineering
Arizona State University, USA
salman.manzoor86@gmail.com

Abstract

There is great interest in minimizing the various losses caused by metal contacts in photovoltaic devices, in particular the optical and shadowing losses. In this study, a polymeric Polydimethylsulfoxide (PDMS) mold inscribed with a triangular microchannel pattern is used to deposit front metal contacts using a highly conductive, low temperature reactive silver ink (RSI) via capillary action. Fingers deposited with this technique exhibit a high aspect ratio, are optically narrow and ~ 85 % transparent. The resulting effectively transparent metal contacts (ETCs) can redirect incoming solar radiation to the photo-active area of the solar cell and mitigate parasitic absorption as well as shading losses. The use of RSI for the development of (ETCs) at low processing temperatures makes it possible for optoelectronic devices to include thermally sensitive layers. RSI exhibits conductivity $>10^4$ S/cm which is comparable to that of bulk silver and anneals at ~100°C, making it suitable for devices that require low temperature processing. With the reduction of porosity upon addition of a suitable solvent and increasing compactness of these grid fingers, they have the potential to outperform their low temperature silver paste screen-printed counterparts.

Keywords: solar; photovoltaic; metallization, transparent contacts, reactive ink .

1. INTRODUCTION

Received in abundance by the earth, Solar energy holds great promise for fulfilling the global energy demand, but a few major challenges need to be overcome to make this technology more economically favorable, One such challenge is increasing the overall efficiency of the modules which operate at less than 18%, far below the silicon balance efficiency limit of 29.8% [1]. The overall solar cell efficiency is affected by many factors, among which losses at the front surface metal contacts play a critical role [2]. Losses in output power of the solar cell at the front metal grid are classified into four types i.e. 1) losses attributed to the internal resistance of the metal electrode 2) losses from the contact resistance between the metal grid and emitter 3) losses due to current flowing through emitter causing emitter resistance and 4) shading losses due to aspect ratio of the front metal contacts which are highly reflective in most cases [3]. In silicon solar cells, screen printed silver contacts carry out charge transport but there is an approximate 4% to 10% loss of incident light because of the shading effect from the metal fingers [4]. These losses can be mitigated to some extent by either modifying the cell design,

changing the scheme of the front contact, or utilizing light management external to the cell. Metal contact design modifications include use of fractal contacts ,transparent conductive oxides (TCOs) [5]- [6], or triangular contacts with high aspect ratio [7], [8].TCOs mitigate optical losses by ommiting the metal but are expensive and face intrinsic parasitic absorption along with low sheet conductivities. Furthermore, in large scale devices, the high photocurrents require metal grid fingers in order to achieve low resistance. These metal fingers lead to further optical losses due to geometric shading [9]. In conventional solar cells with rear and front contacts, a measurable fraction of the incident solar power is lost immediately at the front contact through either absorption, as in transparent conductive oxides or due to reflection at the metal fingers.

Effectively transparent contacts (ETCs), which are high aspect ratio triangular cross-section contacts, have the ability to reflect incident light directly on to the absorber layer in the solar cell, demonstrating over 99% reduction in reflective losses as well as excellent sheet conductivity [1].

These microscale contacts are placed closely together or apart, according to the diffusion length of the device material. c [8] increasing the short circuit current density and mitigating the losses due to parasitic absorption and reflection. With the conventional techniques, such dense spacing of grid fingers would lead to high shading losses, however, the high aspect ratio and triangular cross-section if the ETCs reflects all incident light to the absorber layer [7], [8], demonstrating >85% effective transparency using the reactive silver ink.

In this study, we explore the possibility of using a low temperature reactive silver ink synthesized by a modified Tollen's method [10] with high conductivity and > 20% silver loading. The ink was used to deposit effectively transparent contacts (ETCs) on bare and FTO coated glass slides. Triangular cross-section microchannel grooves, that are 5.6 μm wide, 9.5 μm deep and ~75 μm apart (Fig. 1) were inscribed on to polydilmethylsiloxane (PDMS) using a silicon master mold developed using two photon lithography [11].

So far, the ETCs have been tested on Silicon heterojunction solar cells, bifacial solar cells and perovskites [4], [8], [9] but not on textured Silicon solar cells. Using this design, the fraction of area required by the macroscopic grid fingers can be reduced further on macroscale solar cells and modules compared to conventional designs. Moreover, the ETCs may be used in tandem solar cell architectures along with other optoelectronic devices [9].

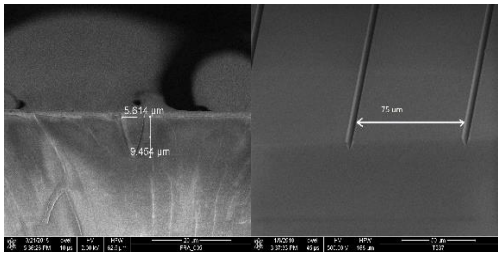

Fig.1. Scanning electron microscope images of a) Cross-section of PDMS stamp with triangular grooves prepared using master mold prepared by two photon lithography b) pitch of the metal finger grid design (~75 μm).

2. Experimental Section

2.1 Synthesis of the Reactive Silver Ink RSI

was synthesized by adding 1g of silver acetate into 2.5 mL aqueous ammonium hydroxide (32%) followed by vortex mixing until the salt was dissolved at room temperature. 0.2 mL of formic acid was then added dropwise with constant vortex mixing after each drop. The change in color of the solution from light brown to greyish black indicates reduction of silver ions to large particles of silver. This solution was kept undisturbed for around 12 hours to allow the larger particles of Ag to settle out and then filtered using a 0.22 μm syringe filter, resulting in a clear ink solution containing 22wt% silver [10], [12]. Thermogravimetric analysis of the ink was carried out at 90ºC (curing temperature) for 30 minutes at a ramp rate of 10ºC/ min and the ink showed stable behavior with only a 6.45% loss in weight.

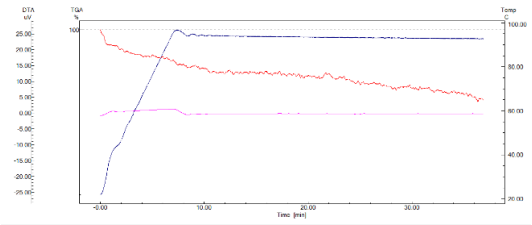

Fig.2. Themogravimetric analysis of RSI carried out at 90ºC for 30 mins at ambient conditions.

Electrical properties of RSI were measured using Hall effect measurements, for which the RSI film was deposited on a bare glass slide by dropping 0.4 mL of ink at 5000 rmp/30 sec. the resistivity of RSI was 4.569×10^{-3} Ω.cm at ambient conditions and the sheet resistivity was measured as 4.569 Ω/ □ , which is quite close to that for commercial silver paste [8].

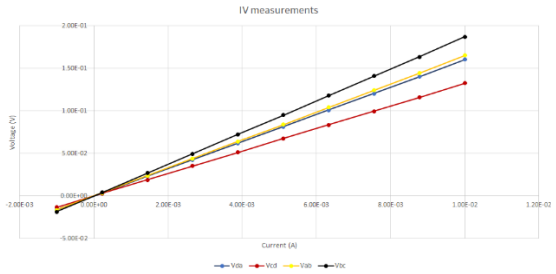

Fig.3. IV curve determined for drop-cast films of RSI using Hall measurements.

2.2 Fabrication of effectively transparent contacts (ETCs)

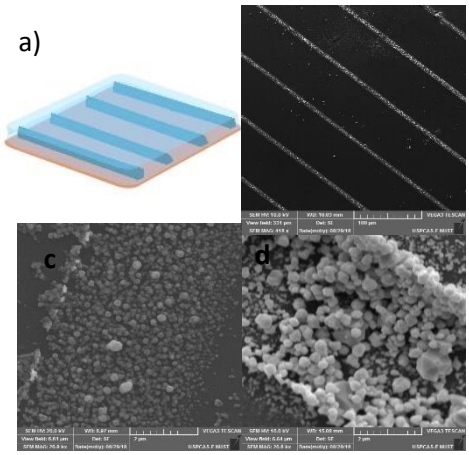

Fig.4. a) Schematic diagram of methodology.

Fig.4. a) Schematic diagram of PDMS stamp with triangular micro-channel grooves, inverted on substrate. Ink is infilled through the sides and travels through the grooves via capillary action. SEM images of b) and c) ETC deposited on glass substrate with undiluted RSI and d) ETC using 1:1 EtOH: Ag ink mixture.

1x1 cm square pieces of the PDMS stamp were cut out and exposed to Medium power Ar/Air plasma (with flow rate 1:2) at ambient temperature. The Plasma treatment facilitates adhesion between the PDMS stamp and substrate [13]. Once removed from the plasma chamber, the stamp must be adhered immediately to a cleaned substrate because the effect of the plasma wears off quickly. After ensuring a tight seal between the PDMS and substrate, RSI (in various concentrations) was infilled from the sides via capillary action. Very minute quantities of ink are required to fill in the stamps, in the µL range. The substrate is heated for 15 minutes at 90ºC and then allowed to cool, before peeling off the stamp.

SEM of the deposited was carried out at 10 kV for the ETCs deposited using RSI in various ratios. The samples were sputtered with gold initially to form a conductive layer. Two samples were analyzed, ETCs formed using undiluted RSI (Fig.4. b and c) and the other using 1:1- EtOH:Ag ink (Fig.4.d). There was a clear difference between the particle size in both the samples. When cured at higher temperature (90 ºC -100 ºC), the ink forms highly porous structures that are discontinuous due to the formation of large pockets as the solvent evaporates since the reduction reaction is favored by higher thermal energy. The viscosity of the 1:1-EtOH:Ag ink is 3.8 mPa.s and weight percentage of Ag is 11.6% [14] as compared to 22% for the undiluted Ag ink [10]. A 10:1-EtOH:Ag ink was also tested but showed lower wettability and failed to flow into the grooves via capillary action. The boiling point of ethanol is 78.4 ºC, which means that curing the diluted ink at 90 ºC gives only a fraction of milliseconds for the solvent to evaporate, resulting in

higher porosity at higher temperatures [14].

UV-VIS spectroscopy was carried out for transmittance measurements of the deposited contacts and a grid finger transparency > 80% was obtained.

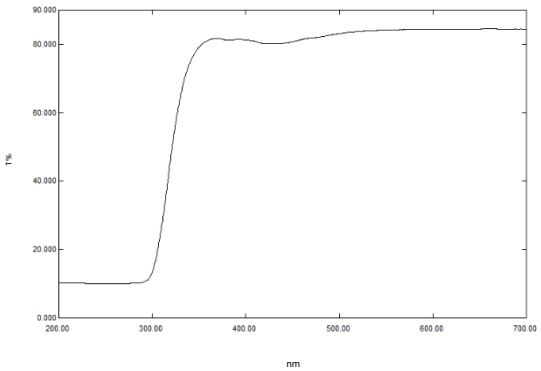

Fig.5.
Transmittance measurements for RSI deposited effectively transparent contacts.

3. RESULTS

Reactive silver ink was used for the deposition of effectively transparent contacts (ETCs) on a glass substrate. These structures exhibited a resistivity equivalent to 4.569x10-3 Ω.cm and sheet resistance of 4.569 Ω/ □ which is impressively similar to that of commercially used screen printed silver paste. Thermogravimetric analysis of the ink shows that it is stable at 90 ºC with only a 6.45% loss in the total weight on the dried ink.

ETCs were deposited on bare glass slide and the structure was analyzed using SEM. ETCs formed using the 1:1 ethanol: Ag ink mixture showed better particle size and continuity, however, both compositions were not able to form the 3-D triangular finger structures as expected, due to poor control over evaporation rates of the solvent.

UV-VIS analysis of the ETCs showed great performance in terms of transmittance, which must be considerably high to allow sufficient light harvesting by the absorber layer.

4. CONCLUSIONS

We have demonstrated that effectively transparent contacts (ETCs) formed using low temperature reactive silver ink (RSI) have the potential to reduce losses incurred due to front grid metallization in solar cells, by minimizing shadowing, reflective and resistive losses. These high aspect ratio Ag fingers placed close enough can TCOs completely. The angle of incidence of these triangular microstructures is such that it maximizes light harvesting. Even though their use is not limited to any particular photovoltaic or optoelectronic device, the use of a low temperature curing ink makes them the ideal candidates for use in thermally sensitive solar cells like perovskites and Si heterojunction cells. The challenge is to optimize the process and find the best suited reactive silver ink composition that can be deposited at lower temperature to suppress formation of large pores during rapid evaporation of solvent upon curing. Once optimized, these low temperature curing ETCs formed using the reactive silver ink have great potential for replacing the conventional screen-printed silver grid fingers in many PV applications

.

NOMENCLATURE

Abbreviations

PDMS	Polydimethylsiloxane
RSI	Reactive silver ink
ETC	Effectively transparent contacts
TCO	Transparent conductive oxides
rpm	rotations per minute

Greek capital symbols

Ω	Ohm

□ square

ACKNOWLEDGEMENTS

The authors acknowledge Rebecca Saive (California Institute of Technology) for providing the polydimethylsiloxane stamp to carry out these experiments. The authors thank Dr. Zak Holman and his research group (Arizona State University) for their incredible help and suggestions regarding the challenges faced in this study.

REFERENCES

[1] P. Jahelka, R. Saive, and H. Atwater, “Total Internal Reflection for Effectively Transparent Solar Cell Contacts,” pp. 1–14, 2016.

[2] Silvaco, “Optimizing Solar Cell Top Metal Contact Design Introduction,” vol. d, no. June, pp. 12–15, 2015.

[3] S. Jeong *et al.*, "Effect of Different Front Metal Design on Efficiency Affected by Series Resistance and Short Circuit Current Density in Crystalline Silicon Solar Cell,” vol. 27, no. 10, pp. 518–523, 2017.

[4] R. Saive, T. C. R. Russell, and H. A. Atwater, “Light Trapping in Bifacial Solar Modules Using Effectively Transparent Contacts (ETCs),” pp. 2–5.

[5] M. A. Aouaj, R. Diaz, A. Belayachi, F. Rueda, and M. Abd-Lefdil, “Comparative study of ITO and FTO thin films grown by spray pyrolysis,” *Mater. Res. Bull.*, vol. 44, no. 7, pp. 1458–1461, 2009.

[6] A. S. Thampy and S. K. Dhamodharan, “Performance analysis and comparison of ITO- and FTO-based optically transparent terahertz U-shaped patch antennas,” *Phys. E Low-Dimensional Syst. Nanostructures*, vol. 66, pp. 52–58, 2015.

[7] R. Saive *et al.*, “Effectively Transparent Front Contacts for Optoelectronic Devices,” pp. 1470–1474, 2016.

[8] R. Saive *et al.*, “Sustainable Energy & Fuels Silicon heterojunction solar cells with e ff ectively transparent front contacts,” *Sustain. Energy Fuels*, vol. 00, pp. 1–6, 2017.

[9] R. Saive, S. Coplin, H. L. Kim, C. H. Van De Stadt, D. Michael, and H. A. Atwater, “Transparent , Conductive and Lightweight Superstrates for Perovskite Solar Cells and Modules,” pp. 1–5.

[10] S. B. Walker and J. A. Lewis, “Reactive Silver Inks for Patterning High-Conductivity Features at Mild Temperatures,” no. I, pp. 2011–2013, 2012.

[11] R. Saive, C. R. Bukowsky, and H. A. Atwater, “Three-dimensional nanoimprint lithography using two-photon lithography master samples,” pp. 1–4, 2017.

[12] S. B. Walker and J. A. Lewis, “Reactive silver inks for patterning high-conductivity features at mild temperatures,” *J. Am. Chem. Soc.*, vol. 134, no. 3, pp. 1419–1421, 2012.

[13] J. Bullock *et al.*, “Microchannel contacting of crystalline silicon solar cells,” pp. 1–8, 2017.

[14] C. Lefky, A. Mamidanna, Y. Huang, and O. Hildreth, “Impact of solvent selection and temperature on porosity and resistance of printed self-reducing silver inks,” *Phys. Status Solidi Appl. Mater. Sci.*, vol. 213, no. 10, pp. 2751–2758, 2016.